Beyond Pairwise Comparisons: A Distributional Test of Distinctiveness for Machine-Generated Works in Intellectual Property Law

Anirban Mukherjee
Hannah Hanwen Chang

26 January, 2026

Abstract

Key doctrines, including novelty (patent), originality (copyright), and distinctiveness (trademark), turn on a shared empirical question: whether a body of work is meaningfully distinct from a relevant reference class. Yet analyses typically operationalize this set-level inquiry using item-level evidence: pairwise comparisons among exemplars. That unit-of-analysis mismatch may be manageable for finite corpora of human-created works, where it can be bridged by *ad hoc* aggregations. However, it becomes acute for machine-generated works, where the object of evaluation is not a fixed set of works but a generative process with an effectively unbounded output space.

We propose a distributional alternative: a two-sample test based on maximum mean discrepancy computed on semantic embeddings to determine if two creative processes—whether human or machine—produce statistically distinguishable output distributions. The test requires no task-specific training—obviating the need for discovery of proprietary training data to characterize the generative process—and is sample-efficient, often detecting differences with as few as 5–10 images and 7–20 texts.

We validate the framework across three domains: handwritten digits (controlled images), patent abstracts (text), and AI-generated art (real-world images). Substantively, we reveal a perceptual paradox: even when human evaluators distinguish AI outputs from human-created art with only ~58% accuracy, our method detects robust distributional distinctiveness. Our results present evidence contrary to the view that generative models act as mere regurgitators of training data. Rather than producing outputs statistically indistinguishable from a human baseline—as simple regurgitation would predict—they produce outputs that are semantically human-like yet stochastically distinct, suggesting their dominant function is as a semantic interpolator within a learned latent space.

---

1 Introduction

Intellectual property law is built on a shared empirical premise: to warrant protection, a work must be meaningfully distinct from a relevant reference class. Whether assessing "novelty" in patent law, "originality" in copyright, or "distinctiveness" in trademark, the inquiry turns on comparing a candidate work against a corpus of existing material—be it prior art, the public domain, or registered marks.[1] While these legal standards differ in threshold and scope, the underlying quantitative question is structurally analogous: does the new work diverge sufficiently from the distribution of existing works to justify an exclusive right?[2]

Yet a fundamental unit-of-analysis mismatch pervades current practice. While inquiries often concern the distinctiveness of a work from a portfolio of works, the available metrics are almost exclusively item-wise and pairwise (Hain et al. 2022; Šavelka and Ashley 2022). For instance, while a court can assess a single painting's features or compare two specific paintings, neither approach directly reveals whether that painting is systematically distinct from an entire portfolio of paintings—or whether one portfolio, such as an artist's body of work, is as a whole systematically distinct from another. Attempts to capture such portfolio-level distinctiveness using existing methods inevitably depend on either qualitative gestalt judgments or *ad hoc* aggregations of pairwise distance metrics—such as mean or maximum similarity—that lack a principled statistical basis (Helmers et al. 2019; Lin et al. 2023).

The emergence of generative AI renders this mismatch intractable. Generative models are stochastic processes with effectively unbounded output spaces (Chesterman 2025). Consequently, comparing only a finite sample of their outputs to a reference class yields an inherently incomplete assessment—whether a sample appears unduly similar or dissimilar to the reference class may be a matter of happenstance rather than a systematic occurrence. Furthermore, the genera-

---

[1] Foundational cases establishing this comparative framework include Graham v. John Deere Co., 383 U.S. 1 (1966) (patent nonobviousness); Feist Publ'ns, Inc. v. Rural Tel. Serv. Co., 499 U.S. 340 (1991) (copyright originality); and Abercrombie & Fitch Co. v. Hunting World, Inc., 537 F.2d 4 (2d Cir. 1976) (trademark distinctiveness).

[2] *See* 35 U.S.C. §§ 102, 103 (2018) (patent); 17 U.S.C. § 102(a) (2018) (copyright); Lanham Act, 15 U.S.C. §§ 1051–1141n (2018) (trademark).

tive process itself is often obscured behind proprietary firewalls. In adversarial litigation, access to training data or model weights is frequently unavailable or contested, preventing direct audits of whether a system is memorizing or interpolating.[3] Finally, the challenge is compounded when AI outputs themselves enter the reference class. When both the candidate source and the reference class possess effectively infinite cardinality, pairwise exhaustion becomes impracticable.

Compounding this structural failure is a collapse of the law's primary instrument of measurement: the human proxy. Courts typically rely on the "ordinary observer" or "person having ordinary skill in the art" to intuit distance between creative works. Yet this reliance has become untenable. Recent empirical work finds that human evaluators distinguish AI-generated images from human creations only marginally better than chance—about 58% for AI-generated art (Silva et al. 2024) and about 62% for photorealistic images (Roca et al. 2025); given recent advances in generative AI, even these figures likely *overstate* current human evaluator performance (Roca et al. 2025, p. 8). Moreover, if ordinary observers struggle, one might expect experts to fare better. They do not. In 2022, Jason Allen's *Théâtre D'opéra Spatial*, created with Midjourney, won the Colorado State Fair's digital arts category; one judge later acknowledged he "didn't realize that it was generated by AI when judging it."[4] In 2025, an entry in Clip Studio Paint's International Illustration Contest won a prize before being withdrawn for using generative AI— despite a multi-stage review that included both detection tools and visual inspection.[5] When even trained evaluators with professional stakes cannot reliably distinguish AI outputs from human creations, the law is left without a stable perceptual yardstick for adjudicating the distinctiveness of machine-generated content.

This paper proposes a distributional alternative: a two-sample test based on maximum mean

---

[3] *See, e.g.*, Andersen v. Stability AI Ltd., No. 3:23-cv-00201, 2023 WL 7132064 (N.D. Cal. Oct. 30, 2023) (granting motions to dismiss in substantial part while allowing direct infringement claim based on training-stage copying to proceed; requiring clearer allegations for output-based and derivative work theories); Getty Images (US), Inc. v. Stability AI Ltd., [2025] EWHC 2863 (Ch) (allowing trademark claims to proceed where plaintiff's watermarks appeared in model outputs; dismissing most copyright claims for lack of UK jurisdiction).

[4] *See* Kevin Roose, *An A.I.-Generated Picture Won an Art Prize. Artists Aren't Happy*, N.Y. Times (Sept. 2, 2022), https://www.nytimes.com/2022/09/02/technology/ai-artificial-intelligence-artists.html.

[5] *See* Press Release, Celsys, Inc., Announcing the Winners of the 44th International Illustration Contest (Aug. 19, 2025) (noting entry withdrawal).

discrepancy (MMD) computed on semantic embeddings.[6] MMD is a kernel-based statistical metric that evaluates samples collectively to determine if they are drawn from the same underlying distribution (Gretton et al. 2012). To capture *meaning* rather than mere surface form, we pair MMD with semantic embeddings—mappings of text or images into high-dimensional vector spaces such that semantic relationships are preserved (Mikolov et al. 2013; Chalkidis and Kampas 2019; Radford et al. 2021). This approach resolves the tripartite challenge identified above: it is *distributional* (solving the unit-of-analysis mismatch), *training-free* (solving the opacity problem), and *objective* (solving the perceptual failure).

Unlike standard machine learning performance metrics (such as Fréchet Inception Distance) that output raw scores (Heusel et al. 2017), we implement MMD as a hypothesis test. By employing permutation testing, we convert the distributional distance into a *p*-value, allowing a fact-finder to determine—at a chosen standard of proof—whether the generative process is statistically distinct from the reference class. This provides a principled way to evaluate whether generative models operate as mere regurgitators of their training data (Bender et al. 2021). If an AI model simply resamples patterns from its training corpus, its output distribution should be statistically indistinguishable from a human reference class.[7] Conversely, if this null hypothesis is rejected, it provides statistical evidence of "interpolative distinctiveness": the model is generating outputs that, while semantically coherent, occupy a distinct topological region of the creative space. While it may retain the capacity for rare memorization, its dominant mode of operation is to function as a semantic interpolator within a learned latent space.

We validate this methodology in three stages. First, we establish statistical robustness using

---

[6]Our framework operationalizes the *empirical* inquiry, not the *normative* legal conclusion. The selection of the relevant reference class—what constitutes the "prior art" or "market"—remains a matter of legal argumentation. Legal doctrines also often incorporate additional factors (e.g., market overlap, commercial purpose, or consumer sophistication). These lie beyond the purely semantic comparison that our metric provides.

[7]If models merely "stitch together" their training patterns, their output distribution should converge to the training distribution in expectation. Support for this line of reasoning can be found in prior investigations. *See, e.g.,* Somepalli et al. (2023) (investigating whether diffusion models merely replicate training data or generate novel compositions, finding that models can regurgitate training examples); *cf.* Goodfellow et al. (2014) (defining the theoretical objective of generative modeling as the minimization of divergence between the model distribution and the data distribution, implying that a model optimizing this objective tends toward statistical indistinguishability from its training set).

the MNIST dataset, confirming the method's sensitivity to known ground-truth differences. Second, we demonstrate domain versatility using patent abstracts, confirming the method's ability to distinguish between technical fields based on textual semantic embeddings. Third, we apply the framework to the AI-ArtBench dataset (Silva et al. 2024), where we reveal a perceptual paradox: even where human evaluators fail to distinguish AI outputs from human art, our test detects robust distributional distinctiveness. We then extend the analysis to recent generative AI models, tracing how the distributional distinctiveness of outputs evolves as generative AI advances. Our finding suggests that these models are not merely replaying prior art but are engaging in interpolative creativity. Practically, we demonstrate that this distinctiveness can be detected with notable sample efficiency—often requiring as few as 5 to 10 samples per group for images, and 7 to 20 for text—offering a scalable evidentiary tool for courts that must evaluate novelty based on limited portfolios.

1.1 Contribution

Our contribution is threefold. First, we introduce a framework that shifts the legal unit of analysis from the *item* to the *process*, resolving the infinite cardinality problem inherent in machine creativity. Second, we provide a sample-efficient implementation that requires no task-specific training, allowing courts and IP offices to assess distinctiveness without requiring access to proprietary model weights or massive training datasets. Third, we provide substantive evidence that the dominant mode of generative models is not mere regurgitation, identifying the phenomenon of "interpolative distinctiveness" where AI outputs are semantically human-like yet stochastically distinct. The remainder of the paper is organized as follows: Section 2 reviews the limitations of current legal and technical metrics; Section 3 details the mathematical derivation of our MMD-based framework; Section 4 validates the methodology using the MNIST dataset; Section 5 extends the validation to the textual domain using patent abstracts; Section 6 applies the framework to the AI-ArtBench dataset to reveal the perceptual paradox; and Section 7 discusses the doctrinal and evidentiary implications for copyright, patent, and trademark law.

2 Distinctiveness in Literature and Practice

Distinctiveness requires a metric that matches the ontology of the subject. Yet, whether in computer science or law, the prevailing tools for measuring distinctiveness remain structurally misaligned with generative AI. These tools attempt to adjudicate *process-level* phenomena using *item-level* evidence, relying on pairwise comparisons and subjective proxies that falter when applied to the effectively unbounded output spaces of machine creativity, while data-dependent metrics are impracticable in litigation where discovery is limited.

In this section, we map this methodological gap. We first critique existing academic metrics—from verbatim memorization checks to pairwise semantic similarity and supervised distinctiveness classifiers—demonstrating how they fail to capture the systemic nature of generative models or require data inaccessible in litigation. We then examine how patent, copyright, and trademark law currently operationalize distinctiveness, showing why human-centric standards cannot scale to the infinite cardinality of machine creativity. Finally, we review the theoretical impasse between regurgitation-based critiques and probabilistic notions of novelty, arguing that this debate remains unresolved precisely because empirical researchers lack a distributional framework capable of distinguishing between mechanical regurgitation and creative interpolation.

2.1 Distinctiveness in the Academic Literature

Research on quantifying the distinctiveness of creative works spans legal scholarship, natural language processing (NLP), and cultural evolution. Prevailing methodologies fall into three primary streams: (1) verbatim memorization metrics, (2) pairwise semantic similarity measures, and (3) supervised proxies for human judgment. These approaches operate fundamentally at the *item* level—scoring specific sentences, images, or marks—rather than at the level of creative processes. A fourth emerging stream—distributional metrics from machine learning—adopts the right structural approach but remains misaligned with legal objectives, prioritizing fidelity over distinctiveness. Consequently, the literature currently lacks a framework capable of quantifying

the divergence of a generative process or the distinctiveness of a set of works from its reference class.

2.1.1 Verbatim Memorization and Exact Matching

Research in AI safety has developed rigorous metrics to detect when models reproduce training data verbatim. For instance, Carlini et al. (2023) quantify memorization by prompting models with prefixes taken from the training set and counting how often the model reproduces long suffixes *exactly*; they also check whether generated continuations appear as verbatim substrings elsewhere in the training corpus. Chang et al. (2023) instead employ membership-inference style tests: carefully constructed cloze prompts over copyrighted books probe whether a model reliably fills in missing passages, revealing when it has effectively memorized the underlying text. The RAVEN framework by McCoy et al. (2023) assesses novelty by measuring, for each generated text, the proportion of structural patterns (e.g., N-grams, syntactic configurations) that do not appear in the training corpus.

While vital for detecting data leakages, these metrics are insufficient for assessing distinctiveness. They are inherently brittle; a model that paraphrases a copyrighted work or mimics an artistic style without exact word-level or pixel-level replication would score as "novel" under these metrics, despite potentially lacking independent creation. Furthermore, they typically require access to the full training corpus—which is often unavailable for proprietary foundation models in litigation or administrative review. Ultimately, they measure *replication*, not *distinctiveness*, and they do so at the level of individual samples rather than the underlying creative process. They cannot determine whether any replication is the system's governing dynamic or merely a statistical anomaly.

2.1.2 Pairwise Semantic Similarity

To capture meaning rather than mere surface form, the dominant methodological paradigm is *pairwise semantic similarity* using semantic embeddings. In this framework, documents or images

are mapped to high-dimensional vectors (using models like BERT for text or ResNet/VGG for images), and distinctiveness is measured as the geometric distance (typically cosine or Euclidean) between a specific candidate work and specific prior art references.

This approach is prevalent in legal informatics and patent analysis. For example, Westermann et al. (2020) use sentence embeddings and approximate nearest-neighbor search to retrieve case-law paragraphs that are semantically similar to a query sentence. In patent and scientometrics, Hain et al. (2022) describe a text-embedding-based method for computing cosine similarity between patents at scale, using these pairwise distances to study technological relatedness and knowledge flows, while Shibayama et al. (2021) use word embeddings to define recombinant novelty scores based on how unusually distant a paper's cited references are from one another. More recently, Lin et al. (2023) use multimodal embeddings to measure patent similarity based on both text and image recognition, and Chiba-Okabe and Su (2024) measure originality as the expected distance between a given image and samples drawn from a baseline distribution of context-conditioned or "generic" images.

However, pairwise methods face a fundamental scaling limitation when applied to generative AI. Assessing an AI model's distinctiveness requires comparing its *generative potential* against potentially infinite sets (e.g., the entirety of prior art). One cannot feasibly compute the distance between every potential AI output and every existing human work. In practice, analysts must rely on finite samples, treating observed distances as deterministic rather than as outcomes of a probabilistic process. Moreover, aggregating pairwise distances—such as taking the mean or minimum distance—yields a statistically impoverished metric as it collapses many pairwise distances into scalars, while also forcing an arbitrary choice among scalars (e.g., mean, median, or variance) that each characterize the distances differently. As Lin et al. (2023) argue, such ad hoc aggregations often depend on arbitrary choices that lack a principled statistical basis (p. 2). This reduction also discards the full distributional structure; without this context, the aggregates lack a null model, leaving courts without a way to determine whether an observed distance is statistically significant (i.e., unlikely to occur purely by chance).

2.1.3   Subjective Proxies and Supervised Classification

Studies have sought to automate distinctiveness judgments by training models to mimic legal decision-makers. In trademark, Adarsh et al. (2024) build a classifier over roughly 1.5 million USPTO applications, using examiner office actions to infer whether a mark was treated as inherently distinctive under the Abercrombie spectrum, and then fine-tune transformer-based language models to predict that label. Similarly, Xu and Ashley (2025) generate synthetic "anchor" marks spanning Abercrombie categories, obtain pairwise distinctiveness judgments for anchor–anchor and anchor–real-mark comparisons from large language models (LLMs), and fit a Bradley–Terry model to these comparisons to derive a continuous "distinctiveness score."

While these methods align closely with legal doctrine, they are inherently limited by their reliance on labeled or pseudo-labeled judgments. First, they are predictive rather than metric: they forecast a *legal conclusion* (e.g., "inherently distinctive" versus "descriptive") rather than quantifying the *empirical distance* between creative processes. Second, they ultimately inherit the limits of human (or human-simulating) perception: Adarsh et al. (2024) use examiner decisions as ground truth, and Xu and Ashley (2025) anchor their scale in Abercrombie-style categories and LLMs trained to emulate legal intuition. This is especially problematic in the context of AI-generated art, where recent empirical work demonstrates that human evaluators distinguish AI-generated images from human art with only approximately 58% accuracy (Silva et al. 2024). If human perception collapses at the item level, supervised models trained to replicate those judgments lose their utility as ground-truth metrics for distinctiveness.

2.1.4   The Distributional Gap

Theoretical legal scholarship has long recognized that distinctiveness should ideally be conceptualized probabilistically. Vermont (2012) argues that copyright's proper domain is *unique* works—those that are "novel and unrepeatable," in the sense that no other creator is likely to independently produce the same work. Byron (2006) develops a probability theory of "copyrightable creativity," under which a work's protectability turns on how unlikely it is to be created given

the constraints of the expressive field. Both accounts treat distinctiveness as a property of an underlying *distribution*: originality becomes "probabilistic uniqueness," the chance that a work would *not* arise again from another draw on the same cultural and technological resources.

However, while legal theory anticipates a distributional framework, existing distributional metrics in machine learning were developed with an inverted objective: establishing fidelity rather than distinctiveness. Metrics such as FID and KID compare the distributions of deep features for real and generated images. They are used as *performance metrics*: lower FID or KID indicates that a generative model more faithfully reproduces the empirical image distribution (Heusel et al. 2017; Bińkowski et al. 2018; Naeem et al. 2020; Wang et al. 2025). While these metrics are undeniably distributional, they function as uncalibrated *scores*: a smaller number is "better," yet there is no principled answer to questions like whether a FID difference of 10 versus 20 corresponds to a meaningful degree of distinctiveness. Crucially, they do not present hypothesis tests; there is no associated null distribution, p-value, or confidence interval, and thus no way to translate a particular score into a statement such as "with 99% confidence, these two generative processes differ."

Recent work on "novelty" pushes closer to the legal question but still falls short of evidentiary needs. Zhang et al. (2024) propose Kernel-based Entropic Novelty (KEN) to quantify *mode-based novelty*, identifying types that occur more frequently in a generative model than in a reference model. Kim et al. (2022) introduce mutual information divergence (MID) to evaluate text–image generative models. While both metrics directly target distributional differences and correlate well with human judgments, they are both scalar metrics. Neither yields a probability or level of confidence that a distribution is distinct from another.

Consequently, a methodological gap remains. There is currently no established framework, particularly in legal or forensic contexts, that combines the *semantic richness* of modern embeddings with the *rigorous hypothesis testing* of statistics. Our proposed framework fills this gap by repurposing kernel methods from performance evaluation to forensic analysis. By wrapping kernel mean embeddings in a two-sample testing procedure, we convert raw distances into p-values,

providing a way to determine—at an explicitly chosen standard of proof—whether two creative processes are statistically distinct.

Thus, we offer a complementary analytical pathway to traditional verbatim memorization checks. While these metrics assess whether *any* specific example of a candidate class or output of a candidate process is similar to a member of a reference class—detecting even rare instances of potential infringement—we assess the *systematic* tendencies of a candidate class or process. A process that is predominantly distributionally distinct may yet produce regurgitative content; conversely, a process that avoids exact verbatim matches may yet produce outputs with substantial similarity to a reference class. Legal adjudication therefore is likely to benefit from both forms of scrutiny: memorization tests to detect specific data leakage, and distributional tests to evaluate the creative independence of the generative process.

2.2 Distinctiveness in Practice

Legal inquiries of novelty, originality, and distinctiveness share a common structure: they are comparative and anthropocentric. In each domain, the law relies on a human proxy—the "person having ordinary skill in the art" (patent), the "ordinary observer" (copyright), or the "reasonable consumer" (trademark)—to perform a pairwise comparison between a specific new work and specific prior art. As we show below, this reliance on pairwise comparisons and human intuition creates a methodological gap when applied to the effectively infinite and non-human output distributions of machines.

2.2.1 Patent

Patent law demands a rigorous, structured comparison between a claimed invention and the "prior art"—a standard codified as novelty and non-obviousness. The Supreme Court formalized this process in *Graham v. John Deere Co.*, establishing a framework that requires the fact-finder to determine "the scope and content of the prior art" and to ascertain the "differences between

the prior art and the claims at issue."[8] This is fundamentally a pairwise exercise: an examiner or court places the claimed invention side-by-side with specific prior art references to determine if the new claim is anticipated or rendered obvious by the old. The benchmark for this measurement is not a quantitative metric, but the PHOSITA—a hypothetical construct used to determine if the difference between the two items would have been "obvious to a person having ordinary skill in the art."[9] This framework has evolved to prioritize functional predictability over rigid rules, yet it remains tethered to human cognition.[10]

In the context of AI, the inquiry has shifted from the distinctiveness of the output to the distinctiveness of the human contribution. In *Thaler v. Vidal*, the Federal Circuit held that an "inventor" under the Patent Act must be a natural person, affirming the rejection of AI systems as inventors.[11] Under current USPTO guidance, inventorship for AI-assisted inventions turns on traditional conception standards: whether a natural person formed a "definite and permanent idea of the complete and operative invention," with AI systems treated as tools analogous to laboratory equipment, effectively rendering the probabilistic novelty (or lack thereof) introduced by AI outputs irrelevant absent significant human contribution.[12] Furthermore, for visual innovations—the domain most relevant to generative art—design patent law employs the "ordinary observer" test established in *Egyptian Goddess, Inc. v. Swisa, Inc.*[13] This test asks whether an ordinary observer, giving such attention as a purchaser usually gives, would find the two designs substantially the same. Like the utility patent framework, this test relies on a gestalt human impression of pairwise similarity rather than a distributional analysis of the design space.

---

[8]383 U.S. 1, 17 (1966) (establishing the framework for non-obviousness).

[9]35 U.S.C. § 103 (2018).

[10]In *KSR International Co. v. Teleflex Inc.*, the Supreme Court rejected rigid tests for obviousness, holding instead that if a combination of known elements yields "predictable results," it lacks the requisite distinctiveness. *See* 550 U.S. 398, 416 (2007).

[11]43 F.4th 1207, 1213 (Fed. Cir. 2022).

[12]*See* Revised Inventorship Guidance for AI-Assisted Inventions, 90 FED. REG. 54,636 (Nov. 28, 2025) (rescinding prior guidance and clarifying that traditional conception standards govern all inventions regardless of AI involvement).

[13]543 F.3d 665, 678 (Fed. Cir. 2008) (en banc) (establishing the "ordinary observer" test for design patent infringement).

2.2.2 Copyright

In copyright jurisprudence, the distinctiveness inquiry operates at two separate stages: the threshold determination of "originality" (validity) and the assessment of "substantial similarity" (infringement). For validity, the Supreme Court in *Feist Publications, Inc. v. Rural Telephone Service Co.* established that originality requires only independent creation and a "modicum of creativity."[14] This threshold is operationally binary, offering no metric for the degree of divergence. By contrast, the standard for *transformative* distinctiveness—relevant to fair use—is substantially more stringent. In *Andy Warhol Foundation v. Goldsmith*, the Supreme Court held that even a work with a distinct aesthetic (e.g., a silkscreen treatment of a photograph) fails to be transformative if it shares the same commercial purpose as the original.[15] This suggests that distinctiveness is not merely a measure of visual difference but also of market function—a nuance that purely geometric metrics may miss.

When measuring infringement, courts employ a bifurcated approach to assess the distance between two specific works. The Ninth Circuit's "extrinsic/intrinsic" test, articulated in *Sid & Marty Krofft Television Productions v. McDonald's Corp.*, exemplifies this pairwise methodology.[16] The "extrinsic" test employs expert testimony to analytically dissect the works and compare objective elements (e.g., plot, themes, dialogue), effectively filtering out unprotectable ideas. If similarity survives this dissection, the "intrinsic" test asks whether an "ordinary reasonable person" would perceive the "total concept and feel" of the works as substantially similar.[17] The Second Circuit's "abstraction-filtration-comparison" test in *Computer Associates International, Inc. v. Altai, Inc.* systematizes this process, filtering out non-distinctive elements before comparing the core of protectable expression.[18] In both frameworks, distinctiveness is measured by the subjective impression of similarity between two works, rather than by any objective measure of a work's standing within a broader portfolio or catalog.

---

[14] 499 U.S. 340, 346 (1991).
[15] 598 U.S. 508 (2023).
[16] 562 F.2d 1157, 1164 (9th Cir. 1977).
[17] *Id.* at 1167.
[18] *See* 982 F.2d 693, 706 (2d Cir. 1992).

Recent cases involving generative AI expose the limitations of these metrics. In *Thaler v. Perlmutter*, affirmed by the D.C. Circuit in 2025, courts applied a strict "human authorship" requirement, refusing to consider the distinctiveness of AI outputs—regardless of their novelty—because they lack a human origin.[19] Conversely, in infringement litigation such as *Andersen v. Stability AI Ltd.*, plaintiffs have struggled to plausibly plead certain theories—such as that AI models contain "compressed copies" of training data or that outputs are infringing derivative works—without showing substantial similarity between specific outputs and specific copyrighted works.[20] Where plaintiffs have succeeded in demonstrating a lack of distinctiveness, it has been through allegations of verbatim or near-verbatim memorization, such as the evidence of text reproduction cited in *The New York Times Co. v. Microsoft Corp.* to demonstrate the model's "regurgitation" of articles (e.g., Exhibit J's red-marked overlaps).[21] This reliance on verbatim metrics confirms that the law currently lacks a tool to measure distinctiveness absent exact replication.

2.2.3 Trademark

Unlike the creativity-focused standards of patent and copyright, trademark distinctiveness is explicitly market-facing: it asks whether a mark can differentiate goods or services in the minds of consumers. Courts operationalize this through a semantic taxonomy known as the "Abercrombie spectrum." Established in *Abercrombie & Fitch Co. v. Hunting World, Inc.*, this framework categorizes marks based on their linguistic relationship to the product: generic, descriptive, suggestive, arbitrary, or fanciful.[22] A mark's placement on this spectrum determines its legal strength. For example, "arbitrary" marks (e.g., "Apple" for computers) are deemed inherently distinctive, while "descriptive" marks require proof of "secondary meaning"—an empirical demonstration that the public associates the term with a specific source.[23] Courts operationalize this inquiry through multi-factor tests, such as the *Polaroid* factors, which explicitly require a pairwise assessment of

---

[19] *See* Thaler v. Perlmutter, 130 F.4th 1039 (D.C. Cir. 2025), *aff'g* 687 F. Supp. 3d 140 (D.D.C. 2023).

[20] *See* No. 3:23-cv-00201, 2023 WL 7132064, at *7–8 (N.D. Cal. Oct. 30, 2023) (requiring plaintiffs to clarify "compressed copies" theory and noting that derivative work claims require substantial similarity allegations).

[21] *See* Complaint at ¶¶ 105–07, Ex. J, N.Y. Times Co. v. Microsoft Corp., No. 1:23-cv-11195 (S.D.N.Y. Dec. 27, 2023).

[22] 537 F.2d 4, 9 (2d Cir. 1976).

[23] *Id.* at 10.

the "similarity of the marks" against specific prior uses.[24] The measurement is primarily conceptual and linguistic, relying on judicial intuition regarding consumer understanding rather than a systematic comparison of the mark against the distribution of existing commercial symbols.

This market-facing inquiry bifurcates when applied to visual trade dress. In *Two Pesos, Inc. v. Taco Cabana, Inc.*, the Supreme Court held that the décor of a Mexican restaurant could be "inherently distinctive" based on a jury's gestalt judgment of its overall look and feel.[25] In contrast, the Court in *Wal-Mart Stores, Inc. v. Samara Brothers, Inc.* ruled that product design (e.g., the cut of children's clothing) can *never* be inherently distinctive and always requires empirical proof of secondary meaning, typically via consumer surveys.[26] These arguments have recently been extended to digital assets. In *Hermès International v. Rothschild* (the "MetaBirkins" case), the court denied summary judgment, and a jury subsequently found that NFT iterations of physical handbags were not distinct enough to avoid confusion, prioritizing consumer perception over the technical novelty of the digital medium.[27] Thus, the law oscillates between subjective "gestalt" impressions and ad hoc empirical data, lacking a unified metric for visual distinctiveness.

Paradoxically, this reliance on cognitive association may enable trademark claims based on AI "hallucinated" marks. In *Getty Images (US), Inc. v. Stability AI, Inc.*, the plaintiff alleged that AI-generated images containing distorted, illegible versions of the Getty watermark nonetheless infringed its trademark.[28] A recent decision by the English High Court in the parallel UK litigation found limited trademark infringement where early versions of Stable Diffusion generated outputs displaying Getty's watermarks, though the court rejected Getty's secondary copyright claims and characterized its trademark findings as "extremely limited."[29] Under traditional confusion analysis, the distinctiveness of the watermark is measured not by its fidelity to the original,

---

[24] Polaroid Corp. v. Polarad Elecs. Corp., 287 F.2d 492 (2d Cir. 1961).

[25] *See* 505 U.S. 763, 773–74 (1992).

[26] 529 U.S. 205, 212–13 (2000).

[27] Hermès Int'l v. Rothschild, 654 F. Supp. 3d 268 (S.D.N.Y. 2023) (denying cross-motions for summary judgment); *see also* Verdict Form at 1, Hermès Int'l v. Rothschild, No. 1:22-cv-00384 (S.D.N.Y. Feb. 8, 2023), ECF No. 146 (finding for Hermès on trademark infringement, dilution, and cybersquatting claims).

[28] Complaint, Getty Images (US), Inc. v. Stability AI, Inc., No. 1:23-cv-00135 (D. Del. Feb. 3, 2023).

[29] Getty Images (US) Inc. v. Stability AI Ltd. [2025] EWHC 2863 (Ch) (Eng.) (finding trademark infringement under ss. 10(1) and 10(2) of the Trade Marks Act 1994 for certain watermark-bearing outputs, while dismissing the s. 10(3) claim and rejecting the secondary copyright infringement theory).

but by its capacity to trigger a cognitive association with the source in the mind of the consumer. If the "hallucination" retains the essential visual characteristics of the mark, it is legally indistinguishable from the genuine article, regardless of its origins.

2.3 Regurgitation vs. Interpolation: Machine Creativity and Distinctiveness

Current intellectual property frameworks operate on a strong presumption against AI distinctiveness, viewing generative systems as tools rather than independent creators. This position relies on the "human authorship" requirement, which posits that AI systems lack the requisite mental conception to produce protectable work. As Ginsburg and Budiardjo (2019) argue, because machines cannot formulate creative plans, they lack the "initiative that characterizes human authorship" and are "closer to amanuenses than to true 'authors'" (p. 349). Under this view, the human programmer or prompter provides the creative rules, and the machine merely executes them (Bridy 2012; Lemley 2023). This doctrinal stance has been formalized in recent administrative and judicial decisions. The U.S. Copyright Office has declined to extend copyright protection to AI-generated images on the grounds that they are not the product of human creative control,[30] and federal courts have affirmed that works generated solely by AI are ineligible for protection.[31] Similarly, patent law now requires that a natural person provide a "significant contribution" to the conception of the invention, effectively treating the AI's output as non-distinctive absent human intervention.[32]

The theoretical underpinning of this legal exclusion is the regurgitation critique. This view posits that LLMs and diffusion models merely stitch together patterns observed in training data without genuine understanding or intent (Bender et al. 2021). Viewed through this lens, AI outputs are "functionally derivative"—operational recombinations of prior art that rely on statistical

---

[30] *See* Letter from U.S. Copyright Office to Van Lindberg, Counsel for Kristina Kashtanova, re: Zarya of the Dawn (Registration # VAu001480196) (Feb. 21, 2023) (canceling original registration and reissuing certificate excluding AI-generated images).

[31] *See* Thaler v. Perlmutter, No. 23-5233 (D.C. Cir. Mar. 18, 2025).

[32] *See* Inventorship Guidance for AI-Assisted Inventions, 89 FED. REG. 10,043 (Feb. 13, 2024).

correlations rather than original expression. This theory is central to current infringement litigation, where plaintiffs allege that AI models contain "compressed copies" of their training corpora and "regurgitate" memorized content.[33] If the regurgitation critique holds, AI outputs should be statistically indistinguishable from the distribution of works upon which they were trained, representing no meaningful departure from the prior art.

However, a competing theoretical perspective suggests that AI generative processes are fundamentally interpolative, potentially yielding "probabilistic novelty." Because generative models map high-dimensional latent spaces to output spaces, they do not simply retrieve existing data points but interpolate between them, often building internal representations of the underlying concepts (Bubeck et al. 2023). Consequently, the resulting outputs are almost always structurally distinct from any single training example. Indeed, the phenomenon of "hallucination" or "confabulation"—where models generate plausible but non-factual content—serves as evidence that the system is diverging from its training distribution rather than merely reproducing it (Ji et al. 2023; Mukherjee and Chang 2023). This argument has been deployed in defense of AI training, with developers arguing that because models learn statistical relationships to generate new expression, the outputs are transformative rather than derivative.[34]

Empirical attempts to resolve this tension have reached an impasse. One strand of research supports the regurgitation view, documenting instances where models memorize and reproduce training data verbatim, particularly when prompted with specific prefixes (Chang et al. 2023; Nasr et al. 2023; Diakopoulos 2023). Conversely, other studies utilizing semantic analysis suggest that AI systems can achieve high degrees of structural novelty and systematic generalization that go beyond mere memorization (Lake and Baroni 2023; McCoy et al. 2023; Lin et al. 2024). This apparent contradiction arises in part from methodological limitations: existing studies typically rely on *item-level* metrics—checking for exact string matches or pairwise similarity between specific outputs and specific training examples. These metrics cannot adjudicate the regurgitation-versus-

---

[33] *See, e.g.*, Complaint, *supra* note 21, at ¶¶ 105–07; *Andersen*, 2023 WL 7132064, at *7–8.

[34] *See* Defendant Meta Platforms, Inc.'s Motion to Dismiss, Kadrey v. Meta Platforms, Inc., No. 3:23-cv-03417 (N.D. Cal. Sept. 18, 2023), ECF No. 23.

interpolation debate because they fail to capture the *distributional* nature of the claim: if a model simply regurgitates, its output distribution should converge to the training distribution. If it interpolates, the distribution should shift. Item-level analysis misses this distinction entirely, as it conflates the occasional novel generation of an output similar to a training example with the regurgitative replication of the training example.

2.4   The Case for a Distributional Framework

The foregoing review reveals a tripartite challenge. Academic metrics face a scaling crisis: verbatim checks are too narrow to capture stylistic mimicry, while pairwise semantic comparisons succumb to the "infinite cardinality" of generative output spaces. Legal tests face an adjudicability crisis: doctrines relying on human proxies (the PHOSITA or ordinary observer) are strained as AI outputs become increasingly difficult for humans to distinguish from human work, yet legal institutions lack the resources to audit massive training sets. Theoretical debates face an empirical impasse: the regurgitation critique cannot be adjudicated by item-level analysis, as even a pure regurgitator can occasionally produce a unique sentence by chance. Resolving these challenges requires a metric that is *distributional* (to solve the scaling problem), *semantically aware* (to capture meaning over form), and *sample-efficient* (to be usable in court).

We propose a framework based on MMD as the specific quantitative remedy. MMD evaluates samples collectively to determine if they are drawn from the same underlying distribution, shifting the unit of analysis from the *item* to the *process*. By pairing MMD with semantic embeddings and permutation-based hypothesis testing, we convert raw distributional distances into *p*-values, allowing fact-finders to assess—at a chosen standard of proof—whether two creative processes are statistically distinct.

This formulation clarifies a critical limitation. Formally, we can view the generative output distribution Q as a mixture: $Q = (1 - \epsilon)Q_{novel} + \epsilon P_{training}$, where ϵ represents the rate at which the model regurgitates training examples rather than generating novel outputs. If ϵ is small, the MMD between Q and P will remain high (indicating distributional distinctiveness), effectively

masking the infringing tail. Thus, MMD measures the dominant creative mode $(1 - \epsilon)$, while memorization audits are required to detect and quantify the regurgitative component (ϵ). This mixture formulation explains why both tests are necessary: MMD evaluates whether $Q \neq P$ (process distinctiveness), while memorization audits detect the presence and magnitude of the $\epsilon P_{training}$ component (item-level infringement).

We position this test not as a replacement for memorization audits, but as a necessary counterpart. Because a generative process may be distributionally distinct yet still produce rare instances of verbatim regurgitation, we advocate for a bifurcated inquiry: using MMD to assess process-level distinctiveness, while employing nearest-neighbor audits to detect specific outliers or "needles in the haystack." The next section develops the mathematical foundations of our approach.

3 Method Development

To resolve the unit-of-analysis mismatch identified in Section 2, we must re-conceptualize the object of inquiry. Rather than focusing on individual items, we represent creative sources—whether a human artist or a generative AI model—as "creative processes," treating specific works as samples drawn from the high-dimensional probability distribution characterizing the process. For instance, the corpus of William Shakespeare's works can be understood as realizations of a specific stochastic process, providing an empirical outline of the random variable describing his creativity.

"Distinctiveness," in turn, is not a measure of the geometric distance between two specific works (such as a new work and a specific prior art reference). Instead, it is the statistical divergence between the distributions of the corresponding stochastic processes, P and Q. If the processes are identical, $P = Q$; if they are distinct, $P \neq Q$.

This conceptual shift accounts for the probabilistic nature of creativity. As the "infinite monkey theorem" suggests, distinct processes may occasionally produce the same output: given infi-

nite time, the creative process of Shakespeare and that of a monkey on a typewriter might both output the same sonnet. However, such overlaps become increasingly unlikely as the processes diverge—on average and in finite time, we would expect a monkey to only produce output that vastly differs from a sonnet. Conversely, if an AI model regurgitates Shakespeare, we would expect high-probability regions of their distributions to overlap, and for the AI's outputs to more frequently and more closely resemble Shakespeare's works. Thus, given finite samples of works from two processes, it is the aggregate pattern of pairwise distances—and not any incidental pairwise distances—that reveals distinctiveness; systemic distinctiveness manifests at the distributional level and not at the item level.

To operationalize this inquiry, we propose a statistical framework based on KMEs (for detailed technical derivations and properties, see Gretton et al. 2012; Muandet et al. 2017)[35], MMD, and semantic embeddings. The methodology integrates two complementary strands of research on embeddings. The first discusses more abstract notions of embeddings and establishes formal properties useful for theoretical analysis (Sriperumbudur et al. 2010). The second develops effective semantic embeddings for non-numerical objects, such as text and images (Mikolov et al. 2013). We combine these approaches to create a unified framework for distributional distinctiveness analysis.

Our approach comprises three steps. First, we employ a semantic embedding to map non-numerical data (such as prior art and AI-generated images) into a numerical vector space where distances reflect semantic relationships (Stammbach and Ash 2021). Second, we use the vector representations to construct KMEs, which map the probability distributions of the works into a reproducing kernel Hilbert space (RKHS) of functions. Third, we compute the MMD between these KMEs—a type of integral probability metric (IPM)—to quantify the statistical distance between the creative processes themselves.

---

[35]The mathematics underlying KMEs is complex. We provide a discussion tailored to our specific use; additional details can be found in the referenced works, with an exhaustive presentation in Berlinet and Thomas-Agnan (2004).

3.1 Definitions and Background

Let $X = \{x_1, x_2, \ldots, x_m\}$ be a sample of works drawn from a process with unknown probability distribution P, and $Y = \{y_1, y_2, \ldots, y_n\}$ be a sample of works from another process with unknown probability distribution Q. Our goal is to test the null hypothesis $H_0 : P = Q$ (the distributions of the processes are identical) against the alternative hypothesis $H_1 : P \neq Q$ (the distributions differ).

In the context of intellectual property adjudication, these variables map directly to the evidentiary record. For instance, P may represent the distribution of a relevant Reference Class (e.g., the corpus of prior art in patent, or the market of registered marks in trademark), while Q may represent the Candidate Process (e.g., a specific AI model). Accordingly, X and Y constitute the observed portfolios presented to the fact-finder. The kernel function k, defined below, acts as the formal proxy for the Ordinary Observer or PHOSITA, providing a consistent metric for the semantic similarity between any two individual works.

An RKHS $\mathcal{H}$ is a Hilbert space of functions defined by a positive definite kernel function $k : \mathcal{X} \times \mathcal{X} \to \mathbb{R}$, where $\mathcal{X}$ is the input space (e.g., the space of possible creative outputs). The RKHS is distinguished by the reproducing property: for every function f in the RKHS and every point $x \in \mathcal{X}$, the value of f at x, $f(x)$, is reproduced by the inner product of f with the kernel evaluation function, which is the kernel function centered at x, $k(\cdot, x)$:

$$f(x) = \langle f, k(\cdot, x) \rangle_{\mathcal{H}}.$$

$k(x, \cdot)$ denotes the kernel evaluation function: a function in the RKHS defined by fixing one argument of the kernel, $y \mapsto k(x, y)$. The kernel function provides a way to "probe" the function f at any point x through the inner product. It allows us to represent high-dimensional or even infinite-dimensional feature spaces implicitly, which is a cornerstone of kernel methods in machine learning (Shawe-Taylor and Cristianini 2004; Steinwart and Christmann 2008).

KME leverages the machinery of RKHS to embed probability distributions into a Hilbert space.

Given a probability distribution P and a reproducing kernel k that induces the RKHS $\mathcal{H}$, the KME of P into $\mathcal{H}$, denoted μ_P, is the expected value of the kernel evaluation function over P:

$$\mu_P = \mathbb{E}_{x \sim P}[k(x, \cdot)] = \int_{\mathcal{X}} k(x, \cdot) \, dP(x),$$

where the integral is a Bochner integral.

A KME maps P to μ_P, a function in the RKHS $\mathcal{H}$. If the kernel k is *characteristic*, then this mapping is *injective* (one-to-one). That is, if two probability distributions differ, their KMEs also differ ($P \neq Q \implies \mu_P \neq \mu_Q$). Equivalently, if the mean embeddings are identical, the underlying distributions must be identical ($\mu_P = \mu_Q \implies P = Q$). This builds on the notion that a kernel function measures the similarity between two points in the input space; if the kernel is sufficiently 'rich' (formally, characteristic), the distance between two KMEs strictly corresponds to the distance between the distributions themselves.

An IPM between distributions P and Q is defined as:

$$\text{IPM}(P, Q) = \sup_{f \in \mathcal{F}} \left| \int_{\mathcal{X}} f(x) \, dP(x) - \int_{\mathcal{X}} f(x) \, dQ(x) \right|,$$

where $\mathcal{F}$ is a class of functions.

MMD is a type of IPM where the class of functions $\mathcal{F}$ is the unit ball in the RKHS. The MMD quantifies the distance between P and Q as the distance between their respective KMEs in the RKHS (Gretton et al. 2012):

$$\text{MMD}^2(P, Q) = \|\mu_P - \mu_Q\|_{\mathcal{H}}^2,$$

where $\|\cdot\|_{\mathcal{H}}$ denotes the norm in the RKHS.

3.2 Employing MMD to Measure Distributional Distinctiveness

Suppose two creative processes produce only numerical data. Given samples X and Y from their distributions P and Q respectively, we can compute an *unbiased* empirical estimator of MMD^2:

$$\widehat{\text{MMD}}_u^2(X,Y) = \frac{1}{m(m-1)} \sum_{i=1}^{m} \sum_{\substack{j=1 \\ j \neq i}}^{m} k(x_i, x_j) + \frac{1}{n(n-1)} \sum_{i=1}^{n} \sum_{\substack{j=1 \\ j \neq i}}^{n} k(y_i, y_j) - \frac{2}{mn} \sum_{i=1}^{m} \sum_{j=1}^{n} k(x_i, y_j). \quad (1)$$

This estimator can be computed efficiently using the *kernel trick*, avoiding explicit computation of the feature maps $k(\cdot, x)$.[36] The components of this equation are interpreted as follows:

- $k(\cdot, \cdot)$ is the kernel function.
- x_i and x_j are samples from distribution P.
- y_i and y_j are samples from distribution Q.
- m and n are the sizes of the samples from P and Q, respectively.
- The first term, $\frac{1}{m(m-1)} \sum_{i=1}^{m} \sum_{\substack{j=1 \\ j \neq i}}^{m} k(x_i, x_j)$, is the average of the kernel evaluations over all distinct ordered pairs of samples from P.
- The second term, $\frac{1}{n(n-1)} \sum_{i=1}^{n} \sum_{\substack{j=1 \\ j \neq i}}^{n} k(y_i, y_j)$, is the average of the kernel evaluations over all distinct ordered pairs of samples from Q.
- The third term, $-\frac{2}{mn} \sum_{i=1}^{m} \sum_{j=1}^{n} k(x_i, y_j)$, subtracts twice the average of the kernel evaluations between samples from P and samples from Q.

MMD^2 can be used to establish the distributional distinctiveness of P and Q. Most creative processes, however, do not generate numerical data. Therefore, to apply this framework to non-numerical data (e.g., text, images), we propose mapping all works into a numerical vector space using a machine learning embedding.

Let $\phi_x : \mathcal{X} \to \mathcal{Z}$ represent such an embedding, where $\mathcal{Z}$ is often $\mathbb{R}^d$, d being the dimensionality of the embedding space. The choice of embedding depends on the specific data type (e.g., a text

---

[36]While the population MMD^2 is strictly non-negative, this unbiased estimator can yield negative values in finite samples if the cross-sample similarity exceeds the within-sample similarity due to sampling noise.

embedding for text data, a convolutional neural network (CNN) embedding for images) and the relevant semantic relationships between the data points (e.g., similarity in meaning for text, visual similarity for art).

We propose the compositional structure:

$$\phi(x) = \phi_k(\phi_x(x)), \quad x \in \mathcal{X},$$

where:

- $\phi_x(x)$ is the machine learning embedding of the 'raw' data point x.
- ϕ_k is the feature map defined implicitly by the kernel k in the RKHS.

Proposition 1 establishes the theoretical validity of this approach. It shows that the kernel defined by the compositional structure $k(\phi_x(x_i), \phi_x(x_j))$ is characteristic if the machine learning embedding ϕ_x is injective and if the kernel k in the RKHS is characteristic. That is, if the machine learning embedding ϕ_x preserves the distinctness of inputs (injectivity) and the kernel k is capable of distinguishing distributions in the vector space (characteristic), then the combined framework can reliably detect distributional differences in the original creative works.

Therefore, we can apply our MMD framework to any data type for which a suitable embedding ϕ_x and a suitable kernel k can be found. This estimator is computed by evaluating the kernel function on the embedded data, replacing $k(x_i, x_j)$ with $k(\phi_x(x_i), \phi_x(x_j))$ in Equation 1.

Proposition 1. *Let $\phi_x : \mathcal{X} \rightarrow \mathcal{Z}$ be an injective mapping and $k : \mathcal{Z} \times \mathcal{Z} \rightarrow \mathbb{R}$ be a characteristic kernel on $\mathcal{Z}$. Then the composed kernel $k_\phi : \mathcal{X} \times \mathcal{X} \rightarrow \mathbb{R}$, defined as $k_\phi(x, x') = k(\phi_x(x), \phi_x(x'))$, is characteristic on $\mathcal{X}$.*

Proof. A kernel is characteristic if the map from probability measures to kernel mean embeddings is injective. That is, for any two probability measures P and Q on $\mathcal{X}$, $\|\mu_P - \mu_Q\|_{\mathcal{H}_\phi} = 0$ must imply $P = Q$.

Let P_x and Q_x be probability measures on $\mathcal{X}$. We define their pushforward measures on $\mathcal{Z}$ as $P_z = P \circ \phi_x^{-1}$ and $Q_z = Q \circ \phi_x^{-1}$.

First, we establish that the mapping from measures on $\mathcal{X}$ to measures on $\mathcal{Z}$ is injective. By definition of the pushforward, $P_z(B) = P_x(\phi_x^{-1}(B))$ for any measurable set $B \subseteq \mathcal{Z}$. Applying this to $B = \phi_x(A)$ for some $A \subseteq \mathcal{X}$, we obtain $P_z(\phi_x(A)) = P_x(\phi_x^{-1}(\phi_x(A)))$. Because ϕ_x is injective, $\phi_x^{-1}(\phi_x(A)) = A$, and thus $P_z(\phi_x(A)) = P_x(A)$. If $P_x \neq Q_x$, there exists a set A such that $P_x(A) \neq Q_x(A)$, which implies $P_z(\phi_x(A)) \neq Q_z(\phi_x(A))$, and thus $P_z \neq Q_z$. Equivalently, $P_z = Q_z$ implies $P_x = Q_x$.

Next, we examine the distance between the kernel mean embeddings. The squared MMD distance in the RKHS $\mathcal{H}_\phi$ associated with the composed kernel k_ϕ is:

$$\|\mu_{P_x} - \mu_{Q_x}\|_{\mathcal{H}_\phi}^2 = \mathbb{E}_{x,x'}[k_\phi(x, x')] - 2\mathbb{E}_{x,y}[k_\phi(x, y)] + \mathbb{E}_{y,y'}[k_\phi(y, y')],$$

where $x, x' \sim P_x$ and $y, y' \sim Q_x$.

By substituting the definition $k_\phi(a, b) = k(\phi_x(a), \phi_x(b))$ and applying the change of variables (where $z = \phi_x(x) \sim P_z$ and $w = \phi_x(y) \sim Q_z$), this equates to:

$$\mathbb{E}_{z,z'}[k(z, z')] - 2\mathbb{E}_{z,w}[k(z, w)] + \mathbb{E}_{w,w'}[k(w, w')] = \|\mu_{P_z} - \mu_{Q_z}\|_{\mathcal{H}_z}^2.$$

This establishes an isometry between the embeddings in the two spaces:

$$\|\mu_{P_x} - \mu_{Q_x}\|_{\mathcal{H}_\phi} = \|\mu_{P_z} - \mu_{Q_z}\|_{\mathcal{H}_z}.$$

$\|\mu_{P_x} - \mu_{Q_x}\|_{\mathcal{H}_\phi} = 0$ implies $\|\mu_{P_z} - \mu_{Q_z}\|_{\mathcal{H}_z} = 0$, and therefore $\mu_{P_z} = \mu_{Q_z}$. Since kernel k is characteristic on $\mathcal{Z}$, the equality of mean embeddings $\mu_{P_z} = \mu_{Q_z}$ implies the equality of distributions $P_z = Q_z$. As established, the injectivity of ϕ_x ensures that $P_z = Q_z \implies P_x = Q_x$.

Therefore, $\|\mu_{P_x} - \mu_{Q_x}\|_{\mathcal{H}_\phi} = 0$ implies $P_x = Q_x$, proving that the mapping $P_x \mapsto \mu_{P_x}$ is injective and the composed kernel k_ϕ is characteristic on $\mathcal{X}$. $\qquad\square$

3.3 Hypothesis Testing

In forensic contexts, a raw distance metric is of limited evidentiary value; a score of "0.1" or "100" is meaningless without a baseline for stochastic variation. To render the MMD metric legally actionable, we must determine whether an observed divergence exceeds what would be expected by chance between two samples drawn from the same process.

We therefore frame the inquiry not as a measurement of magnitude, but as a hypothesis test. This approach allows the fact-finder to explicitly set the significance level (α)—the statistical analogue to the legal standard of proof—thereby controlling the risk of a False Positive (Type I error) where a process is incorrectly deemed distinctive.

To test the null hypothesis $H_0 : P = Q$, we use the empirical estimator $\widehat{\text{MMD}}_u^2$ as our test statistic. Because MMD is a measure of distance, the alternative hypothesis $H_1 : P \neq Q$ implies a strictly positive deviation. Therefore, we employ a one-sided (right-tailed) permutation test: we reject the null hypothesis only if the observed statistic is significantly larger than what would be expected by chance. Negative values of the unbiased estimator, which arise solely from finite sampling noise, are consistent with the null hypothesis and do not constitute evidence of distinctiveness.

Algorithm 1 constructs the null distribution of the MMD statistic by repeatedly resampling the pooled data. This process destroys any systematic distributional differences between the two groups while preserving the marginal distribution of the combined data. The "+1" terms in the numerator and denominator of the p-value formula (step 8) ensure exact Type I error control by treating the observed statistic as an additional permutation under the null hypothesis (Phipson and Smyth 2010). We calculate the critical value c_α as the $(1 - \alpha)$-quantile of these permutation statistics. If the observed statistic $\widehat{\text{MMD}}_u^2(X, Y)$ exceeds this threshold—or equivalently, if the p-value is less than the significance level α—we reject the null hypothesis and conclude that the creative processes exhibit statistically significant distributional distinctiveness.

Algorithm 1 Permutation-Based Hypothesis Test for MMD

Require: Samples $X = \{x_1, \ldots, x_m\}$ from distribution P, samples $Y = \{y_1, \ldots, y_n\}$ from distribution Q, kernel function $k(\cdot, \cdot)$, number of permutation iterations R, significance level α.

1: Compute:

$$\Delta_{\text{obs}} \leftarrow \widehat{\text{MMD}}_u^2(X, Y),$$

$$\widehat{\text{MMD}}_u^2(X, Y) = \frac{1}{m(m-1)} \sum_{i=1}^{m} \sum_{\substack{j=1 \\ j \neq i}}^{m} k(x_i, x_j) + \frac{1}{n(n-1)} \sum_{i=1}^{n} \sum_{\substack{j=1 \\ j \neq i}}^{n} k(y_i, y_j) - \frac{2}{mn} \sum_{i=1}^{m} \sum_{j=1}^{n} k(x_i, y_j).$$

2: Pool samples into a single dataset of size $m + n$:

$$Z \leftarrow X \cup Y.$$

3: **for** $r = 1$ **to** R **do**
4:     Randomly permute the pooled sample Z. Let the permuted sample be Z^*.
5:     Partition Z^* into two sets: X_r^* containing the first m elements, and Y_r^* containing the remaining n elements.
6:     Compute the statistic on the permuted partition:

$$\Delta_r^* \leftarrow \widehat{\text{MMD}}_u^2(X_r^*, Y_r^*).$$

7: **end for**
8: Calculate the *p*-value:

$$p \leftarrow \frac{1 + \sum_{r=1}^{R} \mathbf{1}\{\Delta_r^* \geq \Delta_{\text{obs}}\}}{R + 1},$$

    where

$$\mathbf{1}\{A\} = \begin{cases} 1 & \text{if } A \text{ is true} \\ 0 & \text{otherwise} \end{cases}.$$

9: Determine the critical value c_α from the permutation distribution:

$$c_\alpha \leftarrow Q_{1-\alpha}\left(\{\Delta_r^*\}_{r=1}^{R}\right),$$

    where $Q_\gamma(\cdot)$ denotes the γ-quantile of the permutation-based statistics.
10: **if** $\Delta_{\text{obs}} > c_\alpha$ (or equivalently, if $p < \alpha$) **then**
11:     Reject $H_0 : P = Q$.
12: **else**
13:     Do not reject H_0.
14: **end if**

3.4 Stability of MMD Under Approximate Embeddings

Proposition 1 establishes that if the machine learning embedding ϕ_x is injective, the resulting MMD is a valid metric for distributional distinctiveness. Dimensionality reduction necessarily involves information loss, and one might worry that the pigeonhole principle implies distinct inputs must collide when mapped to a lower-dimensional space.

However, in the context of real-world data, the injectivity condition is not a binding constraint. The pigeonhole principle requires more items (inputs) than slots (outputs). In the context of semantic distinctiveness, this condition is rarely met. Digital images occupy a discrete subset of the input space: pixels take integer values (typically 0–255), and the set of images constituting meaningful creative works is a sparse manifold within that space. Meanwhile, the embedding output space, though discrete at the floating-point level, has vast capacity. For a d-dimensional embedding using standard representations, the number of distinct representable vectors is approximately C^d, where C is the capacity of the floating-point format. For a 1024-dimensional embedding, this yields a state space exceeding 10^{5000} distinct vectors—a number exceeding any plausible enumeration of semantically distinct visual configurations. Moreover, contrastive embeddings are trained precisely to preserve distinctions that matter: two works map to similar vectors if and only if they are semantically similar. Consequently, collisions would require two perceptually distinct works to map to bit-identical vectors, an event with negligible probability.

Nevertheless, a practical concern arises from *approximation error*. In forensic contexts, analysts may rely on off-the-shelf foundation models or dimensionally reduced representations to ensure computational tractability. These networks may not exploit their complete theoretical capacity and may map distinct inputs to proximal representations. It therefore becomes necessary to characterize how such item-level approximation errors propagate to the process-level MMD metric.

We treat approximate embeddings as inducing a bounded perturbation of the kernel values. Proposition 2 demonstrates that the squared MMD is Lipschitz-continuous with respect to this

perturbation: if the embedding error is bounded, the resulting error in the distinctiveness metric is also strictly bounded.

Proposition 2 (Stability under Kernel Perturbations). *Let k_ϕ be the "ideal" composed kernel derived from a high-fidelity embedding, and k_d be an approximate kernel derived from a lower-dimensional or approximate embedding. Suppose the approximation error in the kernel evaluation is uniformly bounded by ε, such that:*

$$\sup_{x,x' \in \mathcal{X}} \left| k_d(x, x') - k_\phi(x, x') \right| \leq \varepsilon.$$

Then for any probability measures P and Q, the absolute error in the squared MMD is bounded by 4ε:

$$\left| \mathrm{MMD}_d^2(P, Q) - \mathrm{MMD}_\phi^2(P, Q) \right| \leq 4\varepsilon.$$

Proof. Recall the expansion of the squared MMD:

$$\mathrm{MMD}^2(P, Q) = \mathbb{E}_{x,x'}[k(x, x')] - 2\mathbb{E}_{x,y}[k(x, y)] + \mathbb{E}_{y,y'}[k(y, y')].$$

Let $\delta(x, x') = k_d(x, x') - k_\phi(x, x')$. The difference between the two MMD estimators is:

$$\Delta_{\mathrm{err}} = \mathbb{E}_{x,x'}[\delta(x, x')] - 2\mathbb{E}_{x,y}[\delta(x, y)] + \mathbb{E}_{y,y'}[\delta(y, y')].$$

Applying the triangle inequality and the uniform bound $|\delta(\cdot, \cdot)| \leq \varepsilon$:

$$\left| \Delta_{\mathrm{err}} \right| \leq \left| \mathbb{E}[\delta(x, x')] \right| + 2\left| \mathbb{E}[\delta(x, y)] \right| + \left| \mathbb{E}[\delta(y, y')] \right| \leq \varepsilon + 2\varepsilon + \varepsilon = 4\varepsilon.$$

The factor of four arises because the MMD expansion involves four expectation terms—two within-group terms and one cross-group term (counted twice)—each of which can accumulate error up to ε. $\square$

This result has specific implications for the Gaussian RBF kernel employed in our empirical analysis, defined as $k(z, z') = \exp(-\|z - z'\|^2 / 2\sigma^2)$. The function $f(u) = e^{-u}$ is 1-Lipschitz on

$[0, \infty)$. Therefore, if an approximate embedding distorts the squared Euclidean distance between any two works by at most η, the kernel value is distorted by at most $\eta/2\sigma^2$.

Combining this with Proposition 2, we obtain a specific bound for Gaussian kernels:

$$\left| \text{MMD}_d^2(P,Q) - \text{MMD}_\phi^2(P,Q) \right| \leq \frac{2\eta}{\sigma^2}.$$

This provides a "safety guarantee" for the metric. For kernels bounded in $[0, 1]$ (such as the Gaussian RBF), the squared MMD always lies in the range $[0, 2]$. If the embedding approximation changes pairwise similarities by at most 1% ($\varepsilon = 0.01$), the final distinctiveness score changes by at most 0.04. This ensures the method remains robust even when operating under computational constraints.

Moreover, it is important to note that the permutation-based hypothesis test described in Algorithm 1 retains exact Type I error control regardless of the embedding employed—a critical feature for admissibility. Under the null hypothesis $H_0 : P = Q$, the permutation distribution is constructed from the same kernel k_d used for the test statistic, ensuring that the critical value c_α correctly bounds the false positive rate at level α. The primary consequence of embedding approximation is a potential loss of statistical power: if k_d introduces systematic distortions, the test may require larger samples to detect true distributional differences. The bounds above quantify this trade-off, allowing practitioners to select embeddings that balance computational efficiency against measurement precision.

Beyond computational tractability, there are substantive reasons to consider dimensionality reduction when applying MMD to machine learning embeddings. Conventional embeddings from foundation models—whether text transformers producing 384- or 768-dimensional vectors or vision models producing 1024-dimensional representations—present two practical challenges. First, these embeddings can be sensitive to input noise: minor perturbations in the original data (compression artifacts, watermarks, or sensor noise) may induce disproportionate shifts in the high-dimensional representation. Second, in very high-dimensional spaces, data points become

increasingly sparse—the well-known "curse of dimensionality"—which can degrade the reliability of distance-based statistics. Dimensionality reduction algorithms such as UMAP (McInnes et al. 2018) address both concerns: by projecting embeddings onto a lower-dimensional manifold, they can attenuate the influence of noise while increasing the effective density of observations in the reduced space. In our empirical analyses, we apply UMAP reduction (to 64 dimensions) to the raw embeddings before computing MMD, finding that this improves robustness to perturbations while preserving—and in some cases enhancing—the test's ability to detect genuine distributional differences.

4   Validation: MNIST Handwritten Digits

Before applying our methodology to real-world data, we validate its statistical properties and practical utility in a controlled setting with known ground truth. We use the MNIST dataset of handwritten digits (LeCun et al. 1998), a widely recognized benchmark in machine learning. MNIST comprises 70,000 grayscale images (28×28 pixels) of handwritten digits from 0 to 9, split into a training set of 60,000 images and a test set of 10,000 images (containing approximately 1000 examples per digit class). Each image represents a single digit, providing a convenient ground truth: it is reasonable to treat the class-conditional distributions of the images of different digits as distinct.

To represent the images in a vector space suitable for MMD calculation, we employ a convolutional neural network (CNN) embedding designed for handwritten digit recognition. We use a LeNet-5-style architecture (LeCun et al. 1998), adapted to use ReLU activations, that consists of two convolutional layers with average pooling, followed by three fully connected (dense) layers; we include dropout regularization (rate = 0.1) after the 120-unit layer and after the 84-unit embedding layer. The architecture is summarized in Table 1.

We train the model on the MNIST training set using the Adam optimizer (learning rate = 0.001), categorical cross-entropy loss, and a batch size of 64. To ensure the learned feature space

Layer Type	Output Shape	Parameters
Input	28×28×1	0
Conv2D (6 filters, 5×5 kernel, ReLU)	24×24×6	156
AvgPool2D (2×2)	12×12×6	0
Conv2D (16 filters, 5×5 kernel, ReLU)	8×8×16	2,416
AvgPool2D (2×2)	4×4×16	0
Flatten	256	0
Dense (120 units, ReLU)	120	30,840
Dropout (rate = 0.1)	120	0
Dense (84 units, ReLU; embedding)	84	10,164
Dropout (rate = 0.1)	84	0
Dense (10 units, Softmax)	10	850

Table 1: LeNet-5-style Architecture Details

is robust to input perturbations, we apply data augmentation during training, including random affine transformations and additive Gaussian noise ($\sigma \sim$ Uniform(0, 1.0)). Training employs early stopping (patience = 10 epochs) and model checkpointing (saving the best model based on validation loss calculated on a 10% hold-out split). Our final trained model achieves a test accuracy of 99.1%, indicating that the learned embeddings effectively capture the distinguishing visual features of each digit while remaining relatively invariant to noise.

4.1 MMD Analysis Procedure and Setup

Our validation procedure comprises the following steps:

1. **Embedding Extraction:** We process all MNIST test images, extracting 84-dimensional embeddings from the penultimate dense layer of the trained model and then applying UMAP reduction to 64 dimensions. These embeddings represent each digit as a numerical vector capturing the high-level visual features identified by the network.

2. **Sample Generation:** We perform comparisons for all 10×10 combinations of digit classes. For each comparison, as a negative control, we compare two *disjoint* random subsamples drawn from the *same* digit class (e.g., digit 3 vs. a different set of digit 3s). Here, we expect the MMD statistic to be near zero and the null hypothesis not to be rejected, providing a

baseline for evaluating the method's Type I error rate. As a positive control, we compare two *disjoint* random subsamples drawn from *different* digit classes. To ensure balanced comparisons and maintain computational feasibility for the permutation-based hypothesis testing, we cap sample sizes at 500 embeddings for each distribution.

3. **MMD Calculation and Hypothesis Testing:** For each pair and sample size, we compute the unbiased squared MMD statistic using a Gaussian radial basis function (RBF) kernel.[37] We opt for the Gaussian RBF kernel as it is *characteristic*, ensuring that the test statistic is a proper metric where a distance of zero implies identical distributions (Gretton et al. 2012). For the bandwidth parameter (σ), we implement the median heuristic, setting σ to the median of all pairwise Euclidean distances in the combined sample for that specific comparison. This data-adaptive approach scales the kernel appropriately to the data's dimensionality; we test the sensitivity of our conclusions to this heuristic in ablation studies. We perform the permutation-based hypothesis test described in Algorithm 1, with $R = 500$ permutation iterations and a significance level of $\alpha = 0.01$.

4. **Sample Size Variation and Rejection Rate Estimation:** To evaluate the method's sensitivity and data efficiency, we repeat steps 2 and 3 across smaller sample sizes: 3, 4, 5, 6, 7, 8, 9, and 10. For each digit pair and sample size, we perform 500 independent trials, each involving fresh random sampling and a full permutation test. Averaging the outcomes (reject/fail-to-reject H_0) across these 500 trials provides a robust estimate of the rejection rate (empirical statistical power) for that scenario. We focus on a representative subset of digit pairs that vary in visual similarity—(0 vs. 1), (1 vs. 7), (2 vs. 8), (3 vs. 5), and (4 vs. 9)—to evaluate performance across both easy and challenging comparisons. This systematic exploration helps characterize the minimum data requirements for reliable distribution discrimination.

---

[37]Throughout the empirical sections, we report values of the unbiased squared MMD estimator ($\widehat{\mathrm{MMD}}_u^2$; see Equation 1). For brevity, we denote this quantity as MMD^2 when reporting numerical results.

4.2 Core Results

Figure 1 illustrates the sensitivity of our approach, describing the estimated rejection rate of the null hypothesis ($H_0 : P = Q$) at a significance level of $\alpha = 0.01$ as the sample size per distribution increases. Our results establish high data efficiency. For both visually distinct examples (e.g., 0 vs. 1, 1 vs. 7) and those exhibiting greater visual similarity (e.g., 3 vs. 5, 4 vs. 9), the rejection rate rapidly surpasses the 95% threshold at just $n = 6$ samples per distribution. As the sample size increases from $n = 3$ to $n = 10$, the rejection rates consistently approach 100% for all tested pairs, confirming the method's statistical convergence.
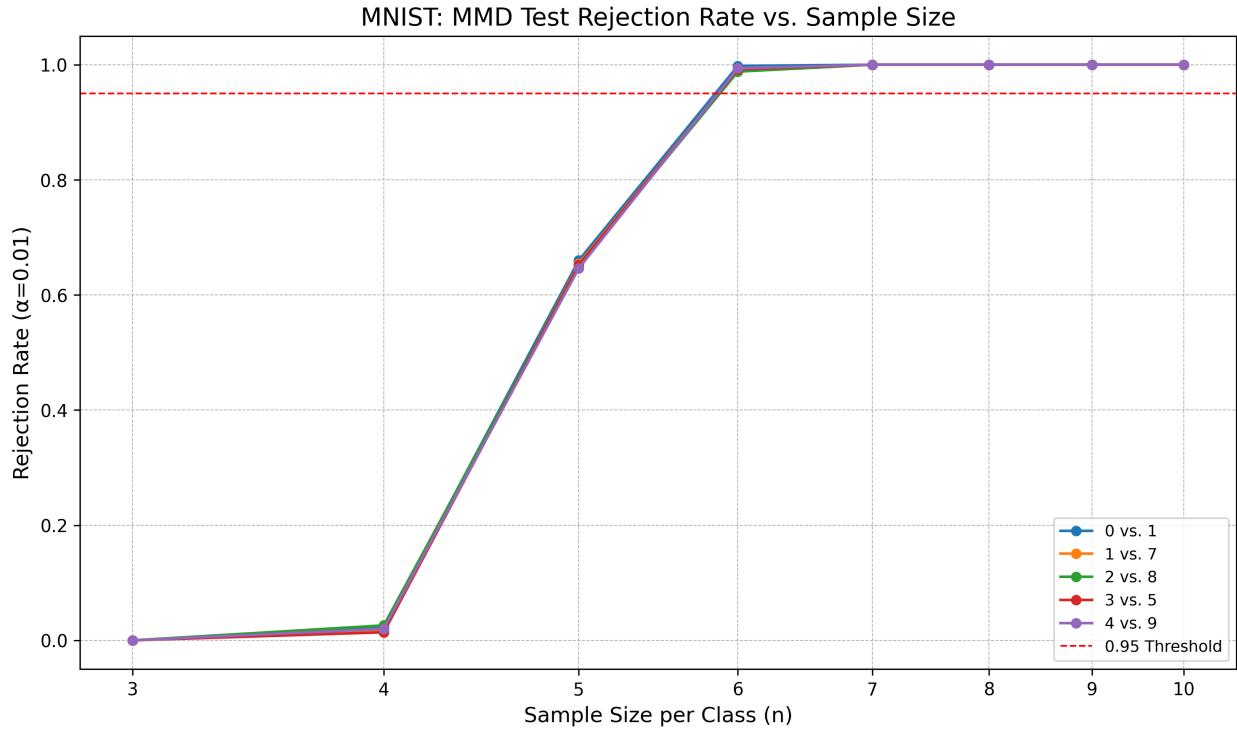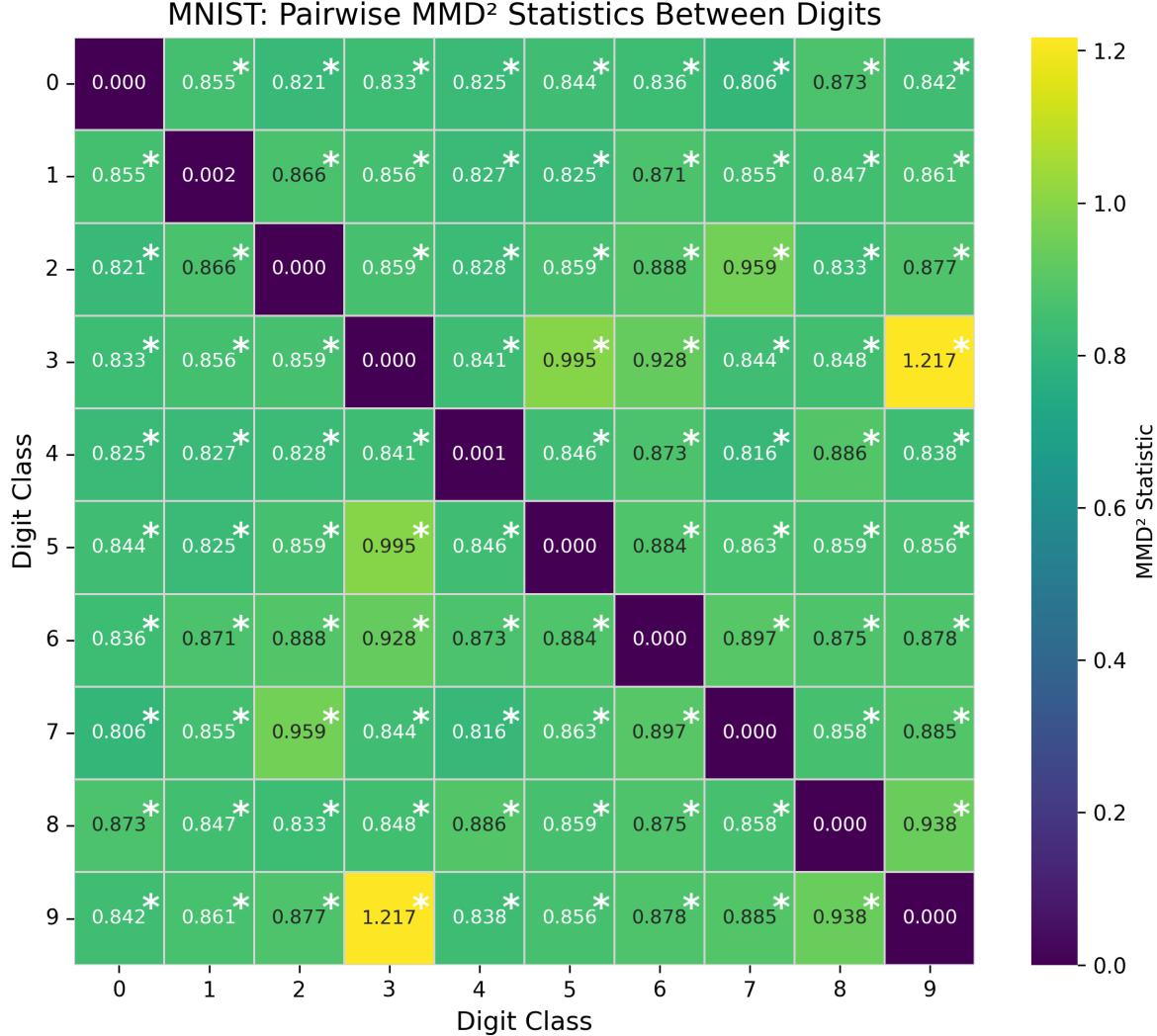

Figure 1: Rejection Rate vs. Sample Size for Selected MNIST Digit Pairs

Note: Each line represents the proportion of null hypothesis rejections ($H_0 : P = Q$) at $\alpha = 0.01$, estimated by averaging results over 500 independent random sampling trials for each sample size and digit pair. The dashed line at 0.95 highlights rapid achievement of high statistical power with very small sample sizes (n=6 for the representative pairs shown).

Figure 2 depicts unbiased squared MMD statistics ($\widehat{\text{MMD}}_u^2$) across all digit comparisons at a sample size of $n = 500$. Diagonal comparisons (negative controls, comparing disjoint samples of the same digit) yield statistics reliably close to zero, consistent with the behavior of the unbiased

estimator under the null. These comparisons yield no rejections of the null hypothesis. In contrast, we reject the null in all 90 off-diagonal comparisons (representing the 45 distinct unordered digit pairs) for $p < 0.01$.

Figure 2: Heatmap of Squared MMD Statistics for All MNIST Digit Pairs (Sample Size $n = 500$). Note: Diagonal cells (negative controls) show near-zero, non-significant MMD values. All off-diagonal cells show statistically significant differences (p < 0.01, marked with *), with MMD magnitudes reflecting the degree of distributional dissimilarity.

This alignment between the quantitative MMD measure and visual dissimilarity indicates that our methodology can reliably and efficiently distinguish between different digit distributions, achieving statistically significant differentiation ($p < 0.01$) with as few as 6 samples per digit class. This level of data efficiency is likely to be particularly valuable in contexts where comprehensive

datasets may be unavailable—such as when evaluating the novelty of a small set of AI-generated works or comparing a new trademark to a limited set of existing marks.
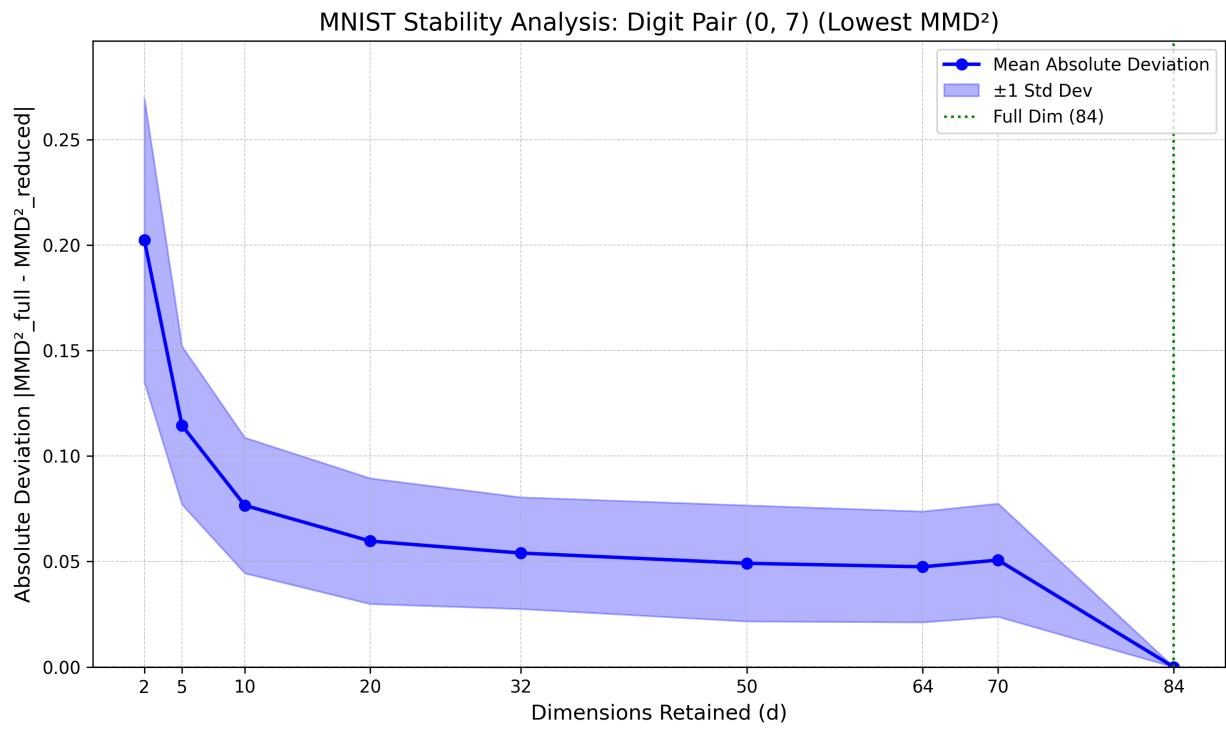
4.3 Metric Stability

While the rejection rates presented above confirm the method's utility in a binary decision context (i.e., distinguishing distinct distributions), forensic applications also require stability in the *magnitude* of the measured distance. If MMD is to serve as a quantitative proxy for distinctiveness, its value should change predictably—rather than erratically—under controlled perturbations to either the embedding representation or the input data itself.

Proposition 2 establishes that the squared MMD is Lipschitz-continuous with respect to bounded kernel perturbations, predicting that the distance estimate should degrade gracefully as information is lost or noise is introduced. We empirically validate this prediction through two complementary analyses: dimensionality reduction (compressing the embedding) and input perturbation (adding noise or watermarks to the raw images).

4.3.1 Dimensionality Reduction

To evaluate how embedding compression affects the MMD metric, we conduct a separate analysis comparing the full 84-dimensional LeNet embeddings to UMAP reductions across a grid of target dimensions $d \in \{2, 5, 10, 20, 32, 50, 64, 70, 84\}$. For each of 100 independent trials, we draw a fixed pair of samples ($n = 50$ per group) and compute the MMD in both the full-dimensional space ($D = 84$) and the reduced space (d) using the same observations. At each d, we recompute the kernel bandwidth σ using the median heuristic. We then record the absolute deviation: $\Delta(d) = |\widehat{\text{MMD}}_{84}^2(X, Y) - \widehat{\text{MMD}}_d^2(X, Y)|$.

Consistent with theoretical expectations, the approximation error decays rapidly as dimensions are added. While the deviation is substantial at extreme compression ($d = 2$), it drops sharply by $d = 10$ (retaining only ~12% of the original dimensions), where the mean absolute error falls below 0.1. By $d = 20$, the error becomes negligible. This confirms that the MMD

Figure 3: Geometric Stability: Absolute Deviation in MMD vs. Retained Dimensions

Note: Mean absolute deviation (with standard deviation error bars) between full-dimensional MMD and reduced-dimensional MMD, computed over 100 independent trials. Consistent with Proposition 2, approximation error decays rapidly as dimensions are added.

metric provides a highly stable measure of distributional distinctiveness even under aggressive dimensionality reduction.

4.3.2 Input Perturbation

To test robustness to data-level corruption, we evaluate how the MMD *statistic itself* responds to systematic and unsystematic image perturbations. We apply Gaussian noise (unsystematic) and grid watermarks (systematic) at varying intensities to images from three digit classes—digits 1, 3, and 8—selected to span a range of visual complexity (simple strokes to complex curves). For each digit, we compare perturbed images against clean images from the same class using a paired design. We parameterize perturbation strength using Signal-to-Noise Ratio (SNR) for Gaussian noise and an analogous Signal-to-Watermark Ratio (SWR) for systematic watermarks, where higher ratios indicate weaker perturbations.

Under the null hypothesis (both sets drawn from the same underlying distribution), we expect MMD to remain near zero when perturbation is minimal. As perturbation intensity increases (SNR or SWR decreases), we expect the MMD to grow, reflecting the increasing distributional divergence between clean and corrupted images.

Table 2 shows that the test statistic is essentially invariant to both noise and watermark perturbations across the entire tested range (SNR and SWR from 25 down to 1). For all three digits, the change in MMD (ΔMMD) between clean and perturbed images remains negligibly small (approximately -0.004, with negative values reflecting variance in the unbiased estimator when distributions are identical). Even at extreme perturbation levels (SNR = 1, where noise standard deviation equals signal standard deviation), the MMD statistic shows no meaningful deviation from zero.

4.4 Inferential Robustness

In a legal context, the dispositive question is not merely whether the measured distance changes, but whether the evidentiary determination is robust to methodological choices. Having estab-

Table 2: Metric Stability: Deviation in Squared MMD (ΔMMD) under Input Perturbation

Digit	Metric	Perturbation Level (SNR or SWR)							
		25	20	15	10	5	3	2	1
Gaussian Noise (SNR)									
1	ΔMMD	−0.005	−0.005	−0.005	−0.005	−0.004	−0.004	−0.004	−0.004
3	ΔMMD	−0.004	−0.004	−0.004	−0.004	−0.004	−0.004	−0.004	−0.004
8	ΔMMD	−0.004	−0.004	−0.004	−0.004	−0.004	−0.004	−0.004	−0.004
Watermark (SWR)									
1	ΔMMD	−0.005	−0.004	−0.004	−0.004	−0.004	−0.004	−0.004	−0.003
3	ΔMMD	−0.004	−0.004	−0.004	−0.004	−0.004	−0.004	−0.004	−0.004
8	ΔMMD	−0.004	−0.004	−0.004	−0.004	−0.004	−0.004	−0.004	−0.004

Note: Change in unbiased squared MMD between clean and perturbed images ($n = 200$). Negative values reflect the variance of the unbiased estimator when distributions are identical or near-identical. The negligible magnitude across all levels confirms geometric stability.

lished that the MMD metric is geometrically stable, we now examine whether the *statistical conclusions*—the decision to reject or fail to reject the null hypothesis—remain reliable under varying conditions. We conduct five ablation studies testing sensitivity to dimensionality, input perturbation, kernel choice, bandwidth, and feature representation.

4.4.1 Dimensionality

We test whether the hypothesis test retains its statistical power when the 84-dimensional LeNet embeddings are reduced via UMAP to $d \in \{10, 84\}$ dimensions. Using digit pair (0 vs. 7), we repeat the permutation test after reducing the 84-dimensional embeddings via UMAP to $d \in \{10, 84\}$ dimensions. Across 100 trials at $\alpha = 0.01$, rejection rates are remarkably stable: at $n = 6$, rejection rates reach 1.00 for both $d = 10$ and full dimensionality ($d = 84$); for $n \geq 7$, rejection reaches 1.00 regardless of compression level. These results confirm that while dimensionality reduction introduces approximation error in the MMD statistic itself (Section 4.3.1), it does not compromise the evidentiary conclusion about distributional distinctiveness.

4.4.2 Input Perturbation

Complementing the metric stability analysis in Section 4.3.2, we examine whether noise and watermarks induce spurious rejections of the null hypothesis. We use a *paired design*: the same images serve as both the clean baseline and the source for perturbation, isolating the effect of the perturbation itself by controlling for content variation. We fit UMAP on the pooled clean and perturbed samples before partitioning to ensure comparison in a common projection space. Under H_0, clean and perturbed versions of the same images should be indistinguishable; rejection indicates the perturbation has created a detectable distributional shift.

Table 3: Inferential Robustness: p-values under Input Perturbation

Digit	Metric	Perturbation Level (SNR or SWR)							
		25	20	15	10	5	3	2	1
Gaussian Noise (SNR)									
1	p-value	1.00	1.00	1.00	1.00	1.00	1.00	1.00	0.97
3	p-value	1.00	1.00	1.00	1.00	1.00	1.00	1.00	1.00
8	p-value	1.00	1.00	1.00	1.00	1.00	1.00	1.00	1.00
Watermark (SWR)									
1	p-value	1.00	1.00	1.00	1.00	1.00	1.00	0.99	0.85
3	p-value	1.00	1.00	1.00	1.00	1.00	1.00	1.00	1.00
8	p-value	1.00	1.00	1.00	1.00	1.00	1.00	1.00	1.00

Note: p-values for MMD test comparing clean digit images against perturbed versions ($n = 200$ per digit, $\alpha = 0.01$). High p-values indicate a failure to reject the null hypothesis, confirming that the method does not produce false positives even in the presence of significant image artifacts.

Table 3 presents the perturbation sensitivity analysis. Remarkably, p-values remain well above the significance threshold ($\alpha = 0.01$) for all digits across the entire range of perturbation intensities tested (SNR and SWR from 25 down to 1). Even at SNR = 1—where noise standard deviation equals the signal standard deviation—p-values remain non-significant for digits 3 and 8, with digit 1 showing only marginal reduction (p = 0.97). This extreme robustness is achieved by computing SNR relative to each digit's own signal variance, ensuring comparable perturbation strength across digits, combined with the noise-augmented training ($\sigma = 1.0$) that produces highly noise-invariant features without sacrificing discriminative accuracy (validation accuracy

99.1%).

The robustness extends to systematic perturbations as well: watermarks at all tested SWR levels (from 25 down to 1) fail to induce spurious rejections for digits 3 and 8, while digit 1 shows slight sensitivity only at the most extreme level (SWR = 1, p = 0.85). This finding has important implications for forensic applications: minor image artifacts—whether from compression, noise, or watermarking—do not compromise the evidentiary conclusion about distributional distinctiveness. The method correctly fails to reject the null hypothesis (that clean and perturbed images come from the same distribution) across virtually all tested perturbation levels.

4.4.3 Kernel Choice

To assess whether the detected distinctiveness depends on the kernel's ability to capture nonlinear structure, we compare the Gaussian RBF kernel against a linear kernel, which is sensitive only to differences in distribution means (centroid shift).

For digit pair (0 vs. 7) at $\alpha = 0.01$ over 100 trials, both kernels achieve comparable inferential performance. At $n = 5$, rejection rates are 0.68 (RBF) and 0.86 (linear); at $n = 6$, they reach 0.98 (RBF) and 1.00 (linear); and by $n \geq 7$, both achieve 1.00. The similar performance of the linear kernel suggests that, for MNIST digits in the learned embedding space, distributional distinctiveness is consistent with substantial centroid shift between digit classes. We retain the RBF kernel for subsequent analyses because of its theoretical guarantees as a characteristic kernel and its greater sensitivity to nonlinear structure in more complex domains (Section 6).

4.4.4 Bandwidth Sensitivity

The Gaussian RBF kernel relies on a bandwidth parameter σ, which we set using the median heuristic. To ensure our conclusions are not artifacts of this specific tuning, we repeat the analysis with σ scaled by factors of 0.5×, 1.0× (baseline), and 2.0×.

For digit pair (0 vs. 7) at $\alpha = 0.01$ over 100 trials, rejection rates are virtually identical across bandwidth settings: at $n = 5$, rejection ranges from 0.68 to 0.75; at $n = 6$, all settings achieve

0.98–1.00; and by $n \geq 7$, all reach 1.00. This "plateau of significance" confirms that the detected distinctiveness is a genuine property of the underlying distributions rather than a brittle artifact of hyperparameter optimization.

4.4.5 Representation

Finally, we test whether the learned embedding is necessary for reliable distinctiveness detection by comparing MMD tests conducted on raw pixel vectors ($28 \times 28 = 784$ dimensions) versus the 84-dimensional CNN embeddings. Table 4 presents rejection rates for three digit pairs spanning a range of visual similarity.

Table 4: Representation Ablation: Rejection Rates ($\alpha = 0.01$, 100 trials) for Raw Pixels vs. Learned Embeddings

Digit Pair	Raw Pixels (784-dim)		CNN Embedding (84-dim)	
	$n = 6$	$n = 10$	$n = 6$	$n = 10$
1 vs. 7 (visually distinct)	0.93	1.00	0.99	1.00
3 vs. 5 (visually similar)	0.22	0.66	1.00	1.00
4 vs. 9 (visually similar)	0.08	0.37	0.99	1.00

Note: Raw pixels are flattened image vectors. CNN embeddings are 84-dimensional features from the trained LeNet-5 penultimate layer. Rejection rate (RR) is the fraction of 100 Monte Carlo trials rejecting H_0 at $\alpha = 0.01$.

The results reveal a critical interaction between representation choice and visual similarity. For structurally distinct digits (1 vs. 7), raw pixel representations achieve high rejection rates (0.93 at $n = 6$, reaching 1.00 by $n = 10$), comparable to the learned embeddings. However, for visually confusable pairs (3 vs. 5; 4 vs. 9), raw pixels perform substantially worse, achieving only 0.08–0.22 rejection at $n = 6$ and failing to exceed 0.66 even at $n = 10$. In contrast, the CNN embeddings achieve ≥ 0.99 rejection at $n = 6$ for all pairs. This demonstrates that learned representations are not merely cosmetic improvements but are essential for detecting distinctiveness when the signal resides in higher-order structural features rather than raw spatial patterns. This finding motivates the use of semantic embeddings (CLIP) for the AI Art analysis in Section 6, where the relevant distinctions are stylistic and conceptual rather than pixel-level.

5 Validation: Patent Abstracts and Textual Distinctiveness

While the MNIST study establishes the statistical validity of our framework in the visual domain, a significant portion of intellectual property—particularly patent claims and literary copyright—is textual. To demonstrate the method's versatility, we extend our validation to the domain of natural language. We apply the MMD framework to patent abstracts, testing whether the metric can reliably distinguish between clearly demarcated technical fields defined by the International Patent Classification (IPC) system.

This experiment serves two purposes. First, it validates the use of text-based semantic embeddings (SentenceTransformers) within our distributional framework. Second, it confirms that the method can detect "prior art" boundaries: if the framework functions correctly, it should identify high distributional similarity within a specific technical field (e.g., Chemistry) and high distributional divergence between unrelated fields (e.g., Chemistry vs. Electricity).

5.1 Dataset and Experimental Design

We utilize the *CCDV Patent Classification* dataset, a benchmark corpus derived from USPTO and EPO patent documents. The dataset categorizes patents according to top-level IPC sections. To ensure a rigorous test of distinctiveness, we select three topologically distinct technical fields:

1. **Section A (Human Necessities):** Covering agriculture, food, and personal goods.
2. **Section C (Chemistry):** Covering metallurgy and chemical engineering.
3. **Section H (Electricity):** Covering electronic circuitry and power generation.

We draw 1000 abstracts from each section, using two disjoint halves of 500 for split-half negative controls; cross-section comparisons use 500 per section. To prevent data leakage, we apply strict preprocessing to remove boilerplate header lines containing IPC section identifiers from the text. This ensures that the embedding model relies solely on the semantic content of the technical

description rather than superficial formatting artifacts—a concern analogous to the watermark sensitivity analysis in the MNIST study (Section 4.4.2).

As with the MNIST study, we employ a *split-half negative control.* For each section, we partition the data into two disjoint subsets (e.g., Chemistry$_A$ vs. Chemistry$_B$). We expect the MMD between these subsets to be statistically indistinguishable from zero, while comparisons between sections (e.g., Chemistry vs. Electricity) should yield statistically significant divergence.

5.2   Semantic Text Embeddings

To map these textual descriptions into a numerical vector space, we employ a sentence transformer model, specifically *GIST-small-Embedding-v0* (Solatorio 2024). Unlike traditional keyword-based methods (such as TF-IDF) which measure lexical overlap, this transformer network maps sentences to a 384-dimensional dense vector space such that semantically similar texts are geometrically close. We select this model for its superior signal-to-noise ratio in our MMD framework compared to alternatives such as *all-MiniLM-L6-v2*.

5.3   Results: Technical Distinctiveness

Figure 4 presents the pairwise MMD statistics for the patent sections. The results confirm the method's efficacy in the textual domain. The diagonal elements (negative controls) show negligible MMD values, and the null hypothesis of identical distributions is not rejected in any split-half comparison ($p > 0.01$). This confirms that the metric does not detect differences where none exist.

Conversely, all cross-section comparisons yield highly significant differences ($p < 0.01$). The MMD statistic effectively captures the semantic distance between technical fields. For example, the distance between *Chemistry* and *Electricity* (distinct physical sciences) is robustly detected. This suggests that the framework can effectively map the "topology of prior art," identifying whether a new set of claims falls within the distribution of an existing field or occupies a distinct region.
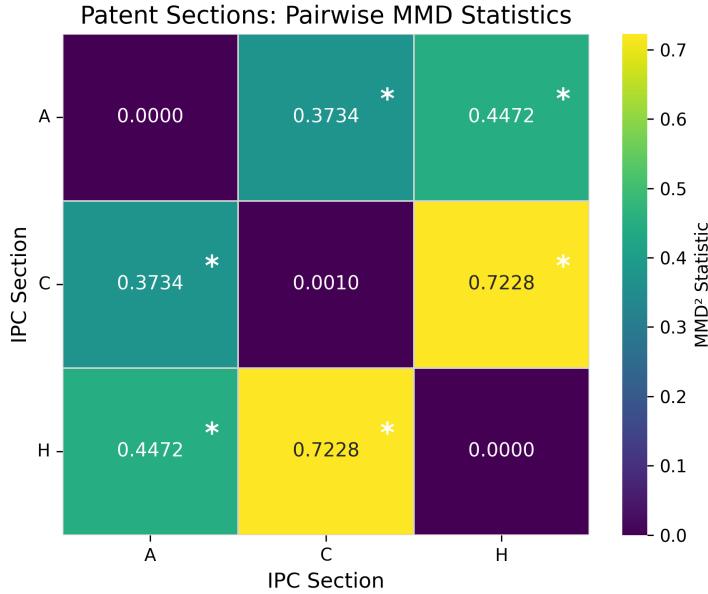
Figure 4: Pairwise MMD Statistics for Patent IPC Sections

Note: Three IPC sections compared: A (Human Necessities), C (Chemistry), H (Electricity). Diagonal cells show split-half negative controls (disjoint samples from the same section); off-diagonal cells show cross-section comparisons. Asterisks indicate statistical significance ($p < 0.01$, permutation test with $R = 500$).

5.3.1 Sample Efficiency in Text

We further evaluate the data requirements for textual analysis. Figure 5 plots the rejection rate of the null hypothesis against sample size.

The results demonstrate reasonable sample efficiency that varies with effect size. The most semantically distinct pair (Chemistry vs. Electricity, $MMD^2 = 0.72$) achieves 95% rejection at $n = 7$; pairs with smaller effect sizes (A vs. H, $MMD^2 = 0.45$; A vs. C, $MMD^2 = 0.37$) require $n = 8$–15 abstracts per group. This finding is relevant for litigation and examination contexts. While not as efficient as the visual domain (where 5–8 samples suffice for MNIST), the ability to reliably distinguish technical fields with 8–15 documents confirms the method is deployable in patent disputes, where examiner searches typically yield dozens of prior art references. Given the algorithmic stability established in the MNIST validation (Section 4.4), we attribute these significant MMD scores to genuine semantic differences rather than artifacts of kernel choice or dimensionality.
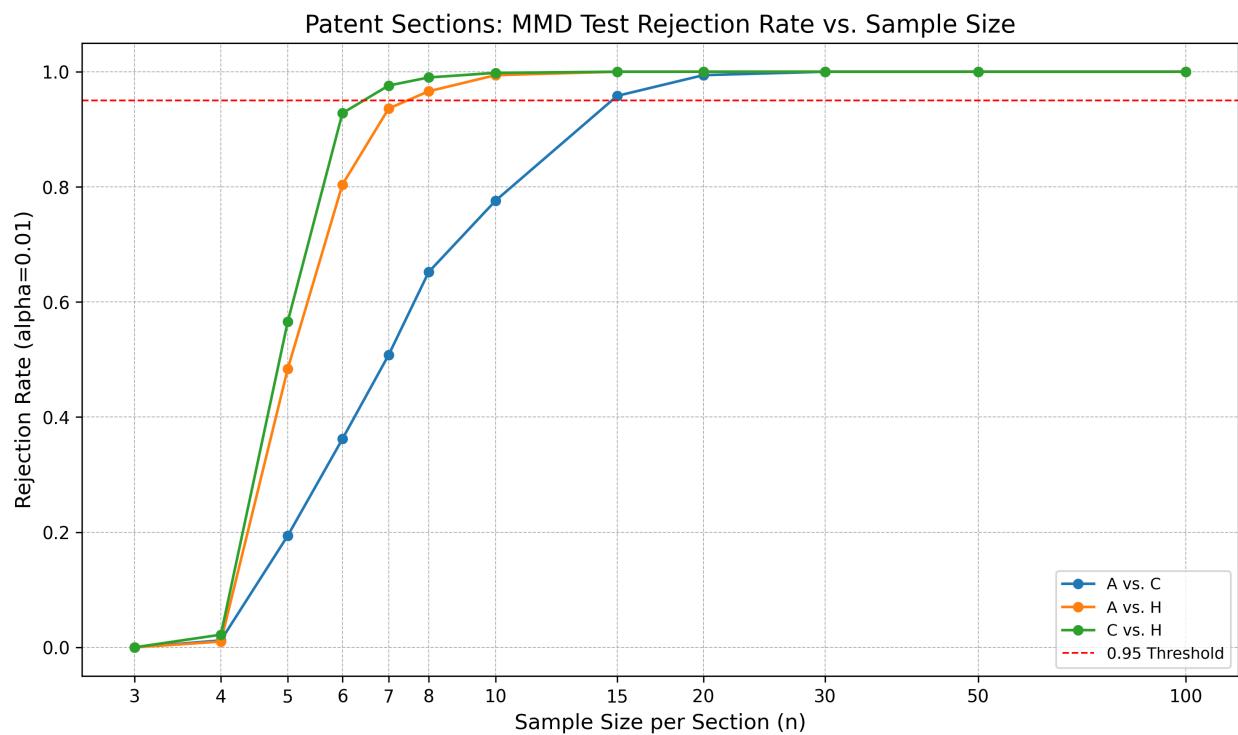
Figure 5: Rejection Rate vs. Sample Size for Patent Section Comparisons

Note: Rejection rate (statistical power) for distinguishing IPC sections at $\alpha = 0.01$ across sample sizes. The most semantically distinct pair (Chemistry vs. Electricity) achieves > 95% power at $n = 7$; pairs with smaller effect sizes require $n = 8$–15 abstracts per group.

6 AI-Generated Art and the Perceptual Paradox

The preceding studies validate our methodology in controlled settings: MNIST provides objective ground truth in the visual domain, and Patent Abstracts demonstrate versatility in text. Creative art presents a more complex challenge: it is subjective, stylistically diverse, and lacks rigid class boundaries. Moreover, human evaluators distinguish AI-generated art from human-created art with only approximately 58% accuracy—barely better than chance. Yet if AI models are genuinely distinct creative processes rather than mere replicators of training data, that distinctiveness should be statistically detectable, even if it eludes direct observation. This section tests whether our MMD framework can resolve this paradox: detecting distributional differences even when human perception fails.

6.1 The AI-ArtBench Dataset and Categories

We employ the AI-ArtBench dataset (Silva et al. 2024), a comprehensive corpus designed to benchmark the detection and attribution of AI-generated art. It comprises 185,015 artistic images spanning ten distinct art styles (including Impressionism, Surrealism, and Art Nouveau). The dataset includes both human-created artworks—60,000 images derived from the curated ArtBench-10 dataset (Liao et al. 2022)—and 125,015 AI-generated images produced using text prompts based on the human artworks. The AI images are generated by two prominent diffusion models:

- **Latent Diffusion (LD):** The original CompVis latent diffusion model, which serves as a foundational architecture for subsequent systems.
- **Stable Diffusion (SD):** A widely deployed latent diffusion model (Rombach et al. 2022), noted for its high-resolution generation capabilities.[38]

We categorize the images into three groups: Human (original human artworks), AI (SD) (images generated by Stable Diffusion), and AI (LD) (images generated by Latent Diffusion). This

---

[38]Silva et al. (2024) refer to this model as "Standard Diffusion" in their dataset and portions of their text, though they also use "Stable Diffusion" interchangeably (e.g., Section 3.1). Their documentation points to the official Stable Diffusion repository, confirming the model identity.

design allows us to test distinctiveness along two axes: the divergence of machine from human, and the divergence of one generative model from another.[39]

This dataset offers a crucial test case because human evaluators can distinguish these AI-generated images from human art with only approximately 58% accuracy (Silva et al. 2024). This near-collapse of perceptual distinctiveness exposes the limits of the "ordinary observer" standard relied upon in copyright and trademark law: if the human eye cannot reliably distinguish the source, legal analysis requires a robust quantitative metric capable of detecting underlying distributional differences that human intuition misses.

In addition, it presents a puzzle: is the AI producing work that *appears* human because it is reproducing memorized training data (pure regurgitation), or because it is interpolating learned patterns to create genuinely novel yet semantically coherent outputs? The perceptual data alone cannot distinguish these possibilities. Our MMD framework allows us to contrast their distributional predictions. If the AI is regurgitating, its output distribution should closely resemble a human-art baseline. If it interpolates, the distributions should diverge.

6.2   Embedding with CLIP

Assessing distinctiveness in the visual arts requires capturing complex stylistic and semantic topologies. Constructing a domain-specific feature extractor for such high-dimensional data requires resource-intensive training on large-scale corpora. However, in actual legal adjudication, courts and IP offices cannot be expected to train bespoke feature extractors for every new dispute. Moreover, such large-scale case-specific training corpora are unlikely to be available. Consequently, a legally viable metric must be "training-free"—capable of evaluating new works immediately using general-purpose semantic knowledge, much like a human adjudicator.

To satisfy these constraints, we employ CLIP (Contrastive Language-Image Pre-training) (Radford et al. 2021). CLIP is a multimodal foundation model pre-trained on massive datasets of

---

[39]We do not observe the full, proprietary training corpora for these diffusion models. Therefore, throughout, we treat the curated human artworks in AI-ArtBench as a proxy for samples from the relevant training distribution (e.g., treating the Impressionist subset of ArtBench-10 as representative of the Impressionist data seen by the models during training).

image-text pairs to align visual and textual concepts. By mapping images into a semantic vector space, CLIP captures high-level features—style, subject matter, and composition—rather than mere pixel-level correlations. This allows us to measure the semantic distance between creative processes without requiring access to the AI's training data or model weights.

Specifically, we use the ViT-H-14-quickgelu variant of CLIP, pre-trained on the dfn5b dataset. We process each image through the encoder to obtain a normalized 1024-dimensional embedding vector. This transforms the raw pixel data into a semantic representation where geometric distance corresponds to conceptual divergence. Relying on a pre-trained foundation model ensures the framework is deployable for "zero-shot" legal analysis, allowing adjudicators to compare new image sources immediately without technical overhead.

6.3 MMD Analysis Procedure and Setup

We apply the MMD framework established in Section 4 to the AI-ArtBench data. We perform comparisons at the category level—comparing Human vs. AI *within* each artistic style—to prevent stylistic confounds from masking or inflating distinctiveness estimates. Therefore, we adapt our sampling strategy to account for stylistic diversity. Specifically, to balance comparisons across artistic movements, we employ *stratified sampling*: we draw 250 images per artistic style for each category (Human, AI-SD, AI-LD), yielding a total dataset of 7,500 images. We pass each sampled image through the pre-trained CLIP encoder to obtain its normalized 1024-dimensional embedding vector and employ UMAP for dimensionality reduction to 64 dimensions. We compute the unbiased MMD statistic using the Gaussian RBF kernel (with median heuristic bandwidth) and assess significance via the permutation test ($R = 500$, $\alpha = 0.01$).

6.4 Core Results: Style-Stratified Distinctiveness

Figure 6 presents per-style MMD heatmaps showing Human vs. AI (SD) vs. AI (LD) comparisons within each artistic style. Across all styles, diagonal elements (negative controls) yield MMD statistics near zero, with all 30 comparisons non-significant at $\alpha = 0.01$, consistent with correct

Type I error control. In contrast, Human vs. AI comparisons yield statistically significant differences ($p < 0.01$) across all ten styles, demonstrating that distributional distinctiveness is a robust feature that persists regardless of artistic movement.
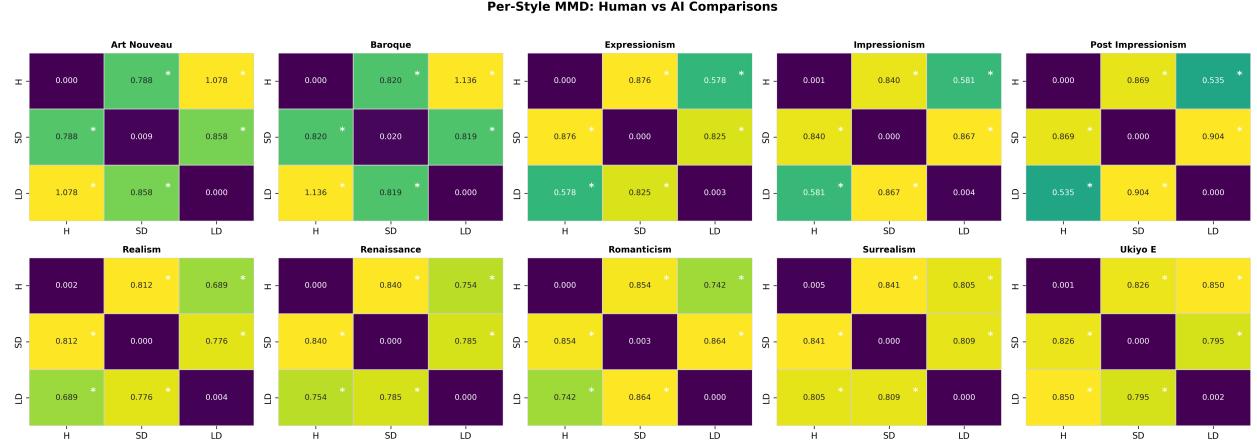

Figure 6: Per-Style MMD Heatmaps: Human vs AI Comparisons Within Each Artistic Movement. Note: Each panel shows Human (H), AI (SD), and AI (LD) comparisons within a single artistic style. Diagonal cells (negative controls) show near-zero MMD values; all 30 diagonal comparisons are non-significant at $\alpha = 0.01$, consistent with correct Type I error control. Off-diagonal cells marked with * indicate statistically significant differences ($p < 0.01$, permutation test with $R = 500$).

Notably, the magnitude of distinctiveness varies substantially across styles, ranging from $\text{MMD}^2 = 0.788$ for Art Nouveau to 0.876 for Expressionism. Figure 7 ranks styles by their Human vs. AI (SD) MMD values, revealing a convergence spectrum: some styles (e.g., those with more constrained compositional conventions) show lower MMD values, indicating that AI outputs more closely approximate the human distribution, while others show higher divergence. This variation is significant—it suggests that the strength of a "distinctiveness" argument may depend on the specific artistic domain under consideration.

However, a raw MMD score is abstract without a baseline. To interpret these magnitudes, we calibrate them against the distances between human art movements calculated within the same embedding space. This establishes an empirical reference scale based purely on the model's topological constraints. Within this framework, closely related schools (Impressionism vs. Realism) yield a noise floor of $\text{MMD}^2 = 0.027$, while historically distinct traditions (Art Nouveau vs. Ukiyo-e) yield a ceiling of $\text{MMD}^2 = 0.859$.
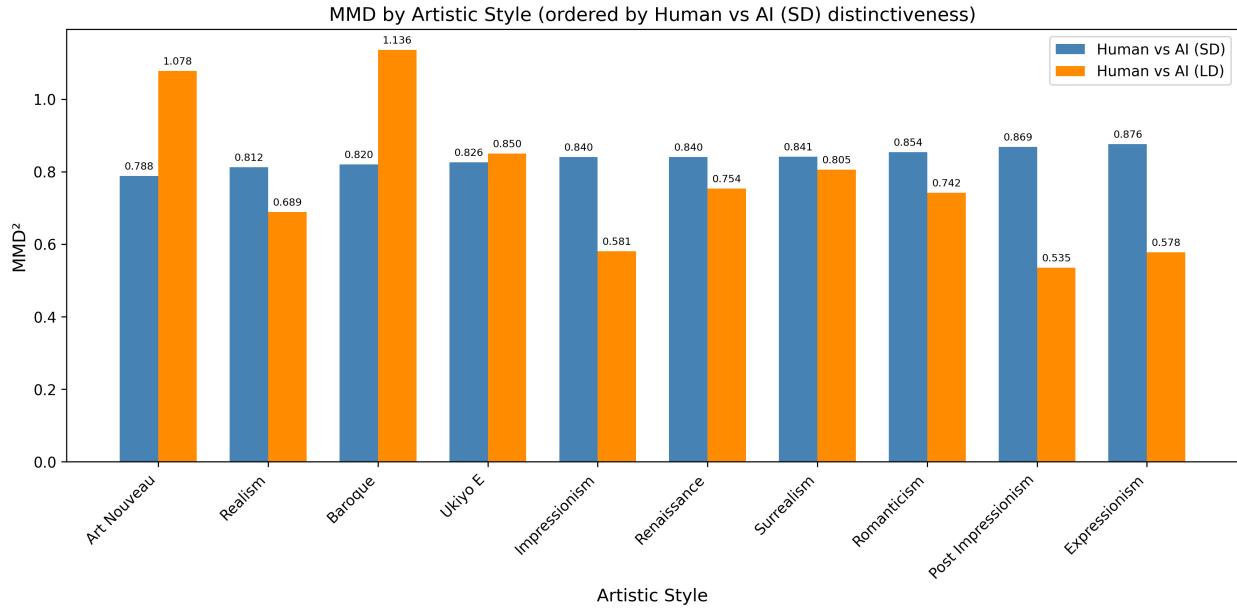
Figure 7: MMD by Artistic Style (ordered by Human vs AI (SD) distinctiveness)

Note: Bars show MMD^2 for Human vs AI (SD) and Human vs AI (LD) within each style. Styles are ordered from lowest to highest Human vs AI (SD) distinctiveness, revealing the convergence spectrum across artistic movements.

Against this scale, the AI outputs do not cluster near the human baseline. The Human-AI (SD) distances (mean 0.837) fall at the upper extreme of the spectrum, comparable to the distance between Art Nouveau and Ukiyo-e. Even Latent Diffusion, the earliest model, achieves a mean distance of 0.775—comparable to the separation between Baroque and Surrealism (0.744). This calibration suggests that the detected distinctiveness is not a statistical artifact of large sample sizes, but a distributional divergence comparable in magnitude to the largest stylistic shifts observed within the human reference set.

Figure 9 and Figure 8 demonstrate the data efficiency of our approach across styles. When comparing human art against Latent Diffusion (LD) outputs, all styles achieve >95% rejection rates with sample sizes of $n = 6$ to $n = 10$ images per source type. There is heterogeneity in styles: "fast-converging" styles (those with lower MMD) require slightly larger samples to achieve high statistical power, while "slow-converging" styles (higher MMD) can be distinguished with fewer samples. A similar analysis comparing human art against Standard Diffusion (SD) outputs shows a faster convergence to high rejection rates. Most styles converge with $n = 6$ images per source

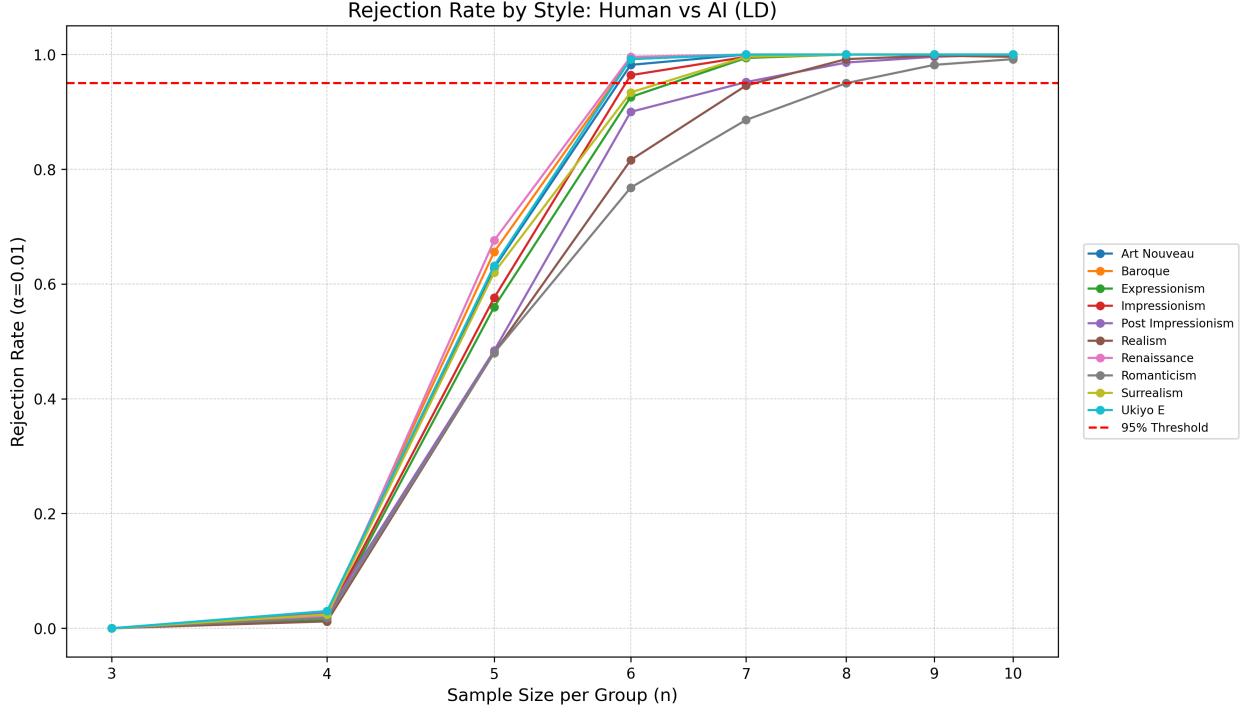type and all styles converge with $n = 7$ images per source type.

Figure 8: Rejection Rate vs. Sample Size by Artistic Style (Human vs Latent Diffusion)
Note: Each line represents the rejection rate for a single artistic style at $\alpha = 0.01$. The dashed line at 0.95 depicts the threshold for reliable detection.

6.5 Robustness of Core Results

We evaluate the stability of these findings through the ablation suite defined in Section 4.4, testing sensitivity to three algorithmic choices under the researcher's control: (1) kernel choice, (2) bandwidth, and (3) dimensionality. For each ablation, we conduct a rejection rate analysis as in Section 6.4, varying the number of samples per group and measuring the proportion of trials that correctly reject the null hypothesis at $\alpha = 0.01$. Table 5 summarizes the results.

Across all three algorithmic dimensions, the detected distinctiveness is robust. For Human vs. AI (SD), kernel choice and bandwidth show uniform convergence by $n = 6$ across all styles, while dimensionality requires larger samples ($n = 17$) due to UMAP's constraint that target dimensions must be less than the number of samples. For Human vs. AI (LD), thresholds are moderately higher—ranging from $n = 6$ to $n = 17$ depending on ablation type and scope—reflecting
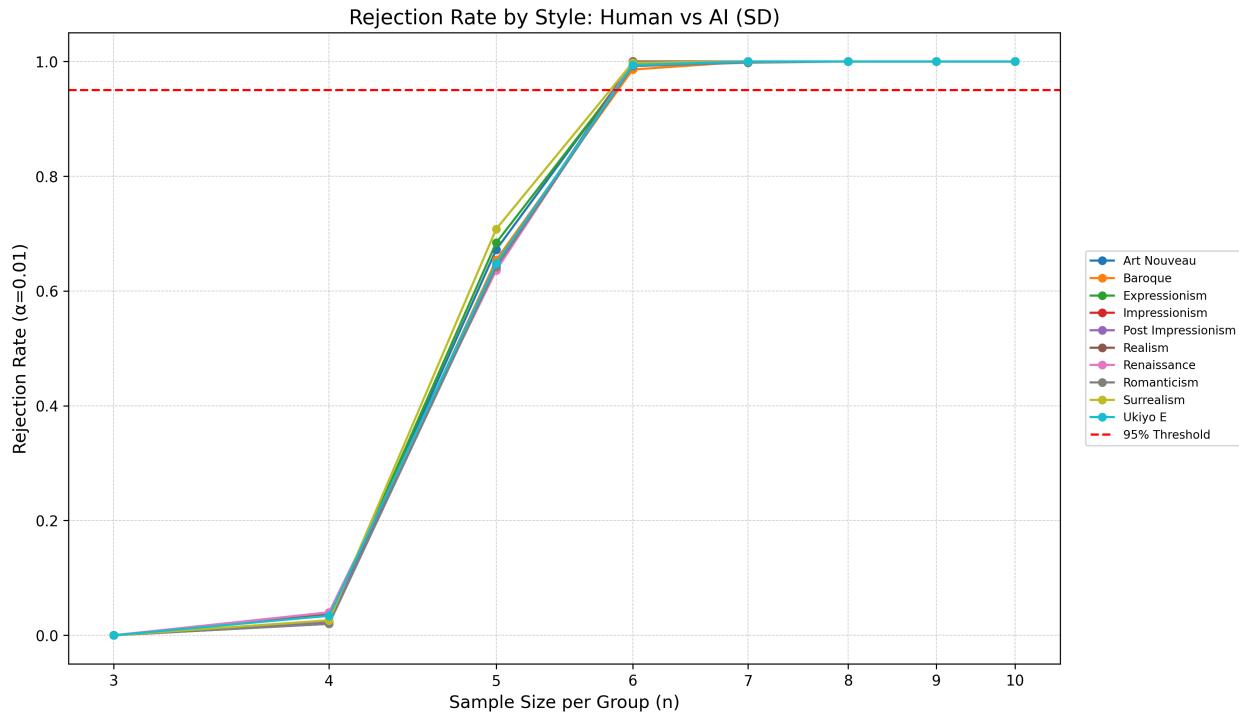
Figure 9: Rejection Rate vs. Sample Size by Artistic Style (Human vs Standard Diffusion)
Note: Each line represents the rejection rate for a single artistic style at $\alpha = 0.01$. The dashed line at 0.95 depicts the threshold for reliable detection.

Table 5: Algorithmic Robustness: Sample Size for 95% Rejection Rate Across Ablation Conditions

Ablation	Scope	Human vs AI (SD)	Human vs AI (LD)
Kernel	Realism	6	10
	Renaissance	6	6
	Post-Impressionism	6	8
	Overall	6	13
Bandwidth	Realism	6	8
	Renaissance	6	6
	Post-Impressionism	6	8
	Overall	6	16
Dimensionality	Realism	17	17
	Renaissance	17	17
	Post-Impressionism	17	17
	Overall	17	9

Note: Each cell reports the sample size (per group) at which the rejection rate first reaches 0.95, taking the maximum across all tested parameter values within each ablation type (RBF/Linear for kernel; 0.5×/1×/2× median for bandwidth; $d \in \{5, 10, 16, 32, 1024\}$ for dimensionality). The higher dimensionality thresholds for Realism, Renaissance, and Overall ($n = 17$) reflect the constraint that UMAP reduction to $d = 32$ dimensions requires at least 34 samples (17 per group).

the somewhat smaller effect size for this earlier generative model (Section 6.5). The Overall LD comparison requires $n = 13$ for kernel ablation and $n = 16$ for bandwidth ablation. These results confirm that the finding of distributional divergence is not brittle; it persists regardless of specific parameter tuning, insulating the method from claims that the results are artifacts of p-hacking or idiosyncratic kernel selection.

We turn finally to input perturbation (Table 6), the most relevant stress test for real-world forensic applications where images may be subject to compression, noise, or watermarking. We compare clean human artworks against perturbed versions of the same artworks; under the null hypothesis, these should be indistinguishable. A robust semantic metric should fail to reject the null hypothesis (i.e., find no difference) unless the perturbation destroys the underlying artistic content.

Table 6: Art Perturbation Robustness: p-values Across Perturbation Levels

		Perturbation Level (SNR or SWR)							
Style	Metric	25	20	15	10	5	3	2	1
Gaussian Noise (SNR)									
Realism	p-value	1.00	1.00	1.00	0.97	0.57	0.07	<0.01	<0.01
Renaissance	p-value	0.94	0.97	0.98	0.69	0.06	<0.01	<0.01	<0.01
Post-Impr.	p-value	1.00	1.00	1.00	0.99	0.86	0.40	<0.01	<0.01
Watermark (SWR)									
Realism	p-value	1.00	1.00	1.00	1.00	1.00	0.99	0.86	0.31
Renaissance	p-value	1.00	1.00	1.00	1.00	1.00	1.00	0.96	0.72
Post-Impr.	p-value	1.00	1.00	1.00	1.00	1.00	1.00	0.98	0.68

Note: p-values for MMD test comparing clean vs. perturbed human artworks ($n = 200$ per style, $\alpha = 0.01$). SNR = Signal-to-Noise Ratio; SWR = Signal-to-Watermark Ratio. Higher values indicate weaker perturbation. Three representative styles from MMD terciles: realism (fast-converging), renaissance (median), post-impressionism (slow-converging).

At typical real-world degradation levels (SNR/SWR ≥ 10), p-values remain well above the significance threshold ($\alpha = 0.01$). This confirms that minor image artifacts do not induce false positives. The test begins rejecting only at moderate-to-substantial perturbation levels: for Gaussian noise, renaissance reaches significance at SNR ≤ 3, while post-impressionism shows the greatest robustness (significant only at SNR = 2). Watermarks show even stronger robustness,

with p-values remaining non-significant across all tested SWR levels for all styles. This establishes the critical forensic property: the metric is sensitive to semantic divergence (the creative process) but invariant to incidental degradation (the file quality).

6.6   Memorization Checks

While distributional distinctiveness characterizes the dominant creative mode, it does not preclude rare item-level memorization. A generative model that is predominantly interpolative may nonetheless produce occasional outputs that closely resemble specific training examples. To address this concern, we complement our distributional analysis with a nearest-neighbor audit using metrics standard in the forensic literature: semantic similarity (CLIP cosine), structural similarity (SSIM), and perceptual similarity (LPIPS).

For each AI-generated image in our dataset (n = 2,500 per model), we identify its nearest neighbor in the human reference corpus (n = 2,500) under three metrics:

1. **CLIP cosine similarity**: Semantic proximity in the CLIP ViT-H-14 embedding space (1024 dimensions). Higher values indicate greater semantic overlap.

2. **SSIM (Structural Similarity Index)**: Pixel-level structural correspondence accounting for luminance, contrast, and structure (Wang et al. 2004). Values range from -1 to 1, with 1 indicating identical images.

3. **LPIPS (Learned Perceptual Image Patch Similarity)**: Perceptual distance computed from deep features (Zhang et al. 2018). Lower values indicate greater perceptual similarity.

To establish a principled detection threshold, we calibrate the metrics against a human baseline. For each human image, we compute its nearest-neighbor similarity to other human images within the same style, establishing the distribution of similarity expected among independent works in a genre. We then set the detection threshold at the 99th percentile of this human-human distribution. Any AI output flagged by this audit thus exhibits similarity to a training example that exceeds 99% of the similarities found between independent human artworks—holding AI to

the same standard as human artists. Under the null hypothesis of no memorization, this threshold yields an expected false-positive rate of 1% (approximately 25 images per model).

Table 7: Item-Level Memorization Audit Results

	Stable Diffusion			Latent Diffusion		
	CLIP	SSIM	LPIPS	CLIP	SSIM	LPIPS
Flagged (n)	0	0	0	0	1	6
Exceedance (%)	0.00	0.00	0.00	0.00	0.04	0.24

Note: Flagged images exceed the 99th percentile of human-human within-style nearest-neighbor similarity. Under the null hypothesis of no memorization, the expected false-positive rate is 1% ($\approx$25 images per model). All observed exceedance rates fall well below this threshold, indicating no systematic memorization. Total samples: 2,500 per AI model.

Table 7 reports the results. CLIP similarity—the metric most sensitive to semantic content— flagged zero images for both models, indicating no high-level conceptual copying. SSIM and LPIPS, which capture lower-level structural and perceptual features, flagged a small number of candidates: 0 images for Stable Diffusion (0.00%) and 7 images for Latent Diffusion (0.28%). Critically, both rates fall well below the 1% false-positive rate expected by chance, providing statistical evidence against systematic memorization.

To adjudicate these flags, we conducted visual inspection of all 7 flagged cases (all from Latent Diffusion). Figures 10, 11, and 12 present these comparisons. In every instance, the flagged AI images depict entirely different subjects from their matched human paintings. For example, Figure 10 shows five AI-generated images flagged against a Correggio religious scene—images that share Renaissance stylistic characteristics (warm color palettes, painterly textures) but lack any compositional or subject-matter overlap. All flags arose from incidental stylistic convergence rather than reproductive memorization.

In sum, the item-level memorization audit detected no credible instances of training-data replication. The few statistical flags represent false positives at threshold boundaries, confirmed by visual inspection to reflect superficial stylistic similarity rather than copied content. Combined with the distributional MMD analysis, these findings establish that text-to-image models generate novel interpolations within the learned manifold rather than regurgitating training examples.

LPIPS Flagged: Human Renaissance and 5 Matching AI (LD) Images

HUMAN
Correggio

AI (LD) #1
Latent Diffusion

AI (LD) #2
Latent Diffusion

AI (LD) #3
Latent Diffusion

AI (LD) #4
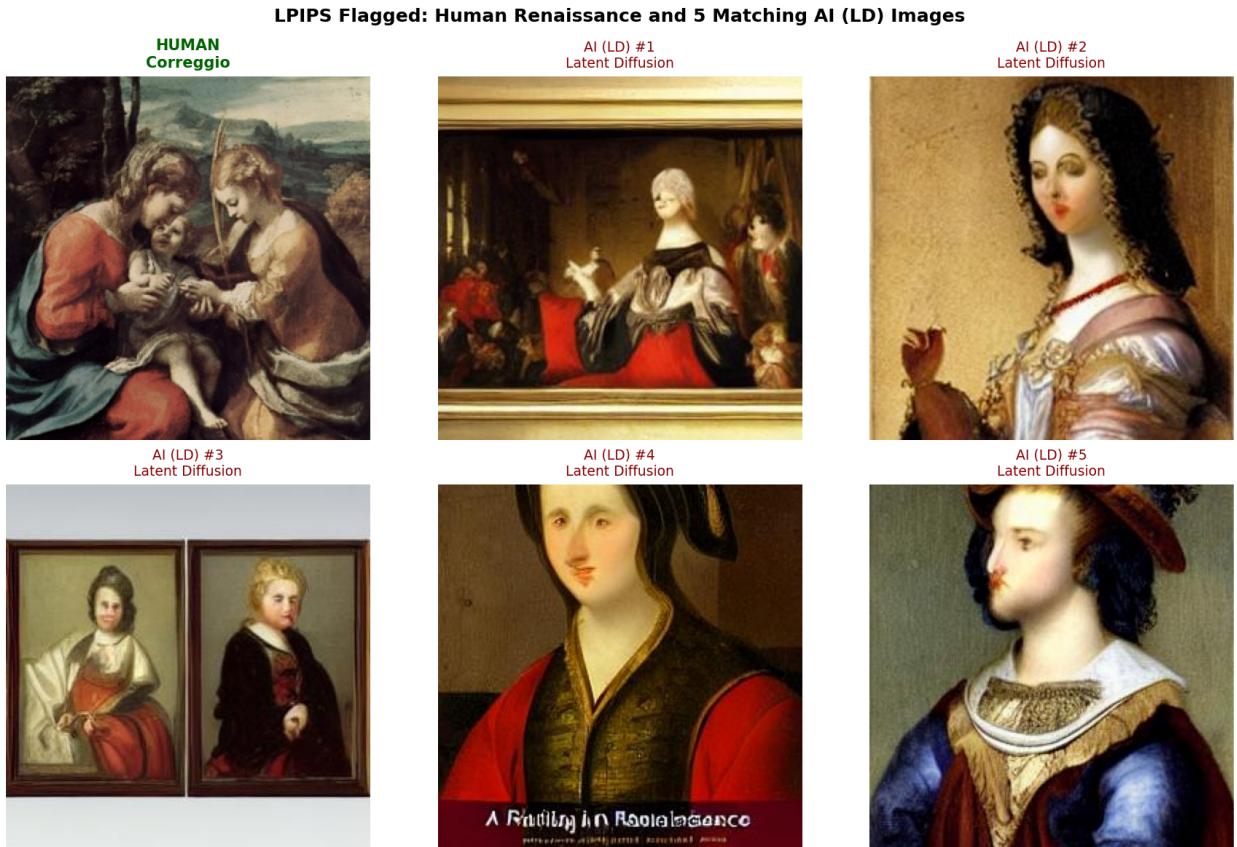Latent Diffusion

AI (LD) #5
Latent Diffusion

Figure 10: LPIPS-Flagged Renaissance Comparisons

Note: Human reference (Correggio, *The Mystic Marriage of St. Catherine*, 1518) and 5 flagged Latent Diffusion outputs. The LPIPS metric detected shared warm color palettes and soft textural qualities characteristic of Renaissance painting. However, subjects differ entirely: the reference depicts a multi-figure religious scene while the AI outputs are predominantly single-figure portraits or framed scenes. Several AI images contain visible text artifacts ("Renaissance Art Style"), a hallmark of early diffusion models that further confirms non-reproductive generation.

LPIPS Flagged: Human Baroque and 1 Matching AI (LD) Image

HUMAN
Anthony Van Dyck

AI (LD) #1
Latent Diffusion

Figure 11: LPIPS-Flagged Baroque Comparisons

Note: Human reference (Anthony van Dyck, *Portrait of Sir John Mennes*, c. 1640) and 1 flagged Latent Diffusion output. The LPIPS metric detected shared warm red and gold color palettes characteristic of Baroque painting. However, the subjects differ substantially: a male portrait in armor versus an ornate framed religious scene. The similarity reflects period-typical color choices rather than content replication.

SSIM Flagged: Human Expressionism and Matching AI (LD) Image
(SSIM=0.657, threshold=0.643)

HUMAN
Edwin Dickinson

AI (LD)
Latent Diffusion

Figure 12: SSIM-Flagged Expressionism Comparison

Note: Human reference (Edwin Dickinson, *An Anniversary*, 1921) and 1 flagged Latent Diffusion output. Despite strikingly different color palettes—the human work is dark and muted while the AI output is vibrant—the SSIM metric flagged this pair based on similar structural density and brushwork patterns. This illustrates how pixel-level structural metrics, which operate on luminance channels, can conflate textural similarity with copying even when semantic content and color are entirely distinct.

6.7 Evolution of Generative Distinctiveness

As text-to-image models become more sophisticated, their outputs converge semantically with real-world images and human art. But does this fidelity arise because the outputs are moving closer to their training samples, or because the models are interpolating more effectively? Put differently: do better outputs reflect better regurgitation or better learning?

To investigate this, we extend our analysis beyond the AI-ArtBench data to include three subsequent generations of diffusion models. Our expanded dataset spans five years of development: Latent Diffusion (Dec 2021), Stable Diffusion v1.4 (Aug 2022), Stable Diffusion XL (Jul 2023), FLUX (Aug 2024), and FLUX-Krea (Jul 2025).[40]
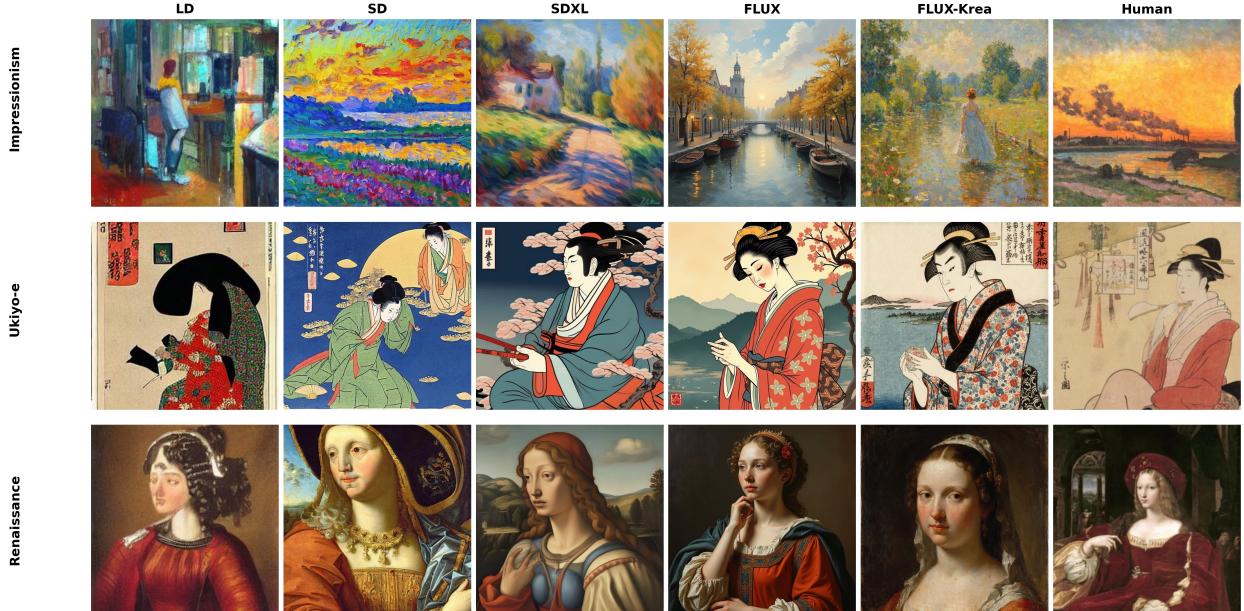

Figure 13: Exemplar Images Across Model Generations and Artistic Styles

Note: Each column represents a model generation, ordered chronologically from Latent Diffusion (LD) to FLUX-Krea, with human originals in the final column for comparison. Rows correspond to three artistic styles (Impressionism, Ukiyo-e, Renaissance) with consistent subject matter.

---

[40]We deliberately employ models within a single architectural lineage rather than comparing across model families (e.g., Midjourney, DALL-E, Imagen) as otherwise we might conflate capability improvements with differences in architecture, training data, and design philosophy; by staying within the Stable Diffusion lineage, we isolate the effect of advancing capability on distributional distinctiveness. This choice also has practical relevance: Stability AI, the developer of Stable Diffusion, is currently a defendant in high-profile intellectual property litigation—including *Andersen v. Stability AI Ltd.* and *Getty Images (US), Inc. v. Stability AI Ltd.*—making our findings directly relevant to the empirical questions at the heart of these disputes.

Figure 13 illustrates the visual progression across model generations. Early models (LD, SD) exhibit visible artifacts, such as blocky textures and inconsistent details. Later generations (SDXL, FLUX) eliminate these flaws but tend toward photorealism, producing outputs that often resemble photographs or 3D renders more than paintings. FLUX-Krea, a fine-tuned variant designed specifically to enhance artistic aesthetics, strikes a balance: it recovers much of the stylistic fidelity while maintaining high coherence.
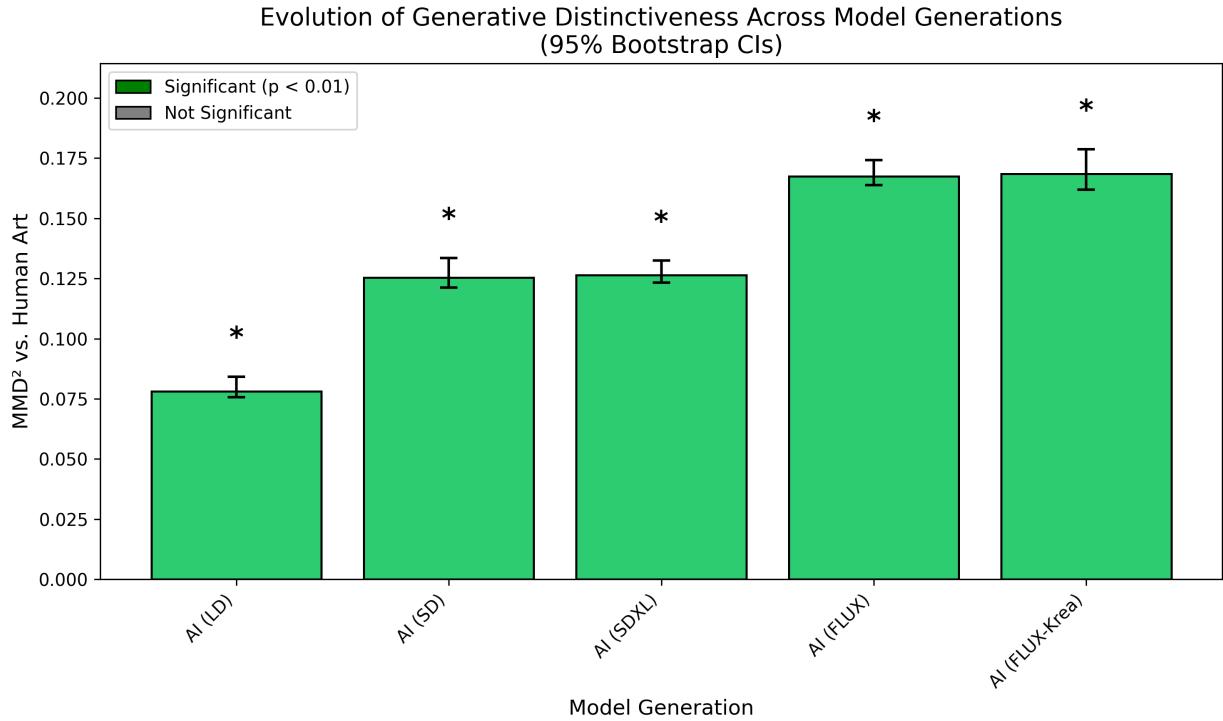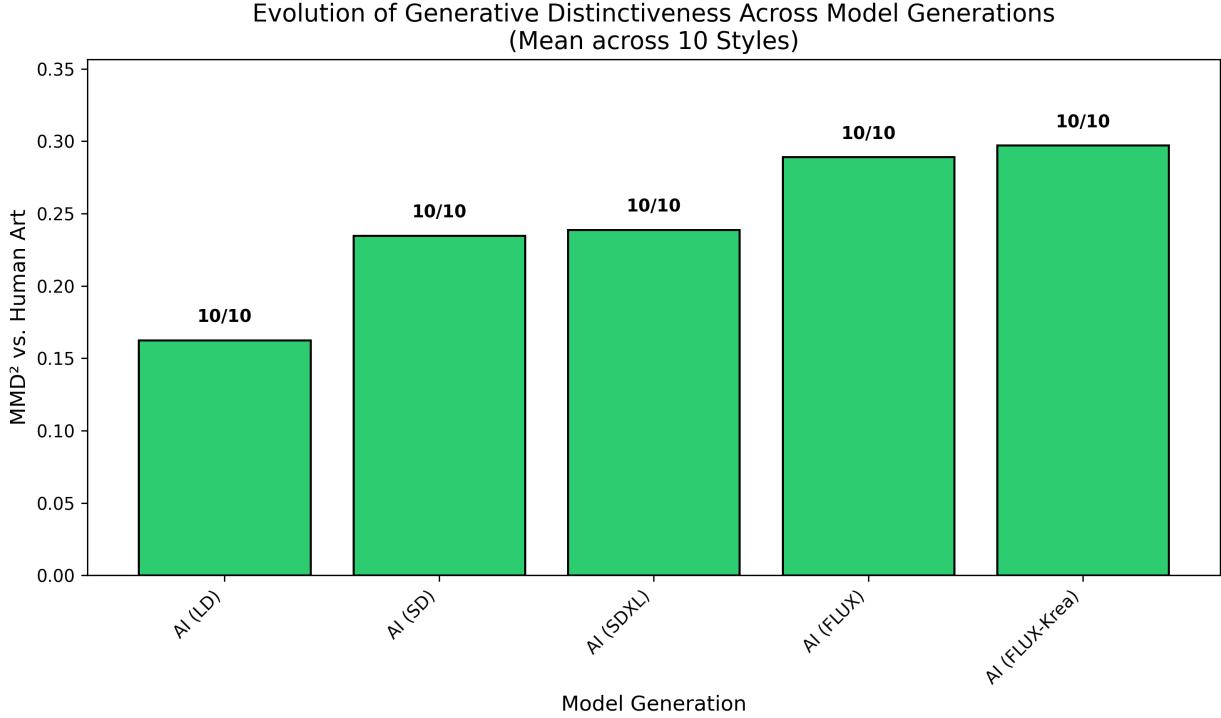

Figure 14: Evolution of Human-AI Distributional Distinctiveness Across Model Generations (Pooled)

Note: MMD^2 between human artworks and outputs from each model generation, pooling across all ten artistic styles. Error bars indicate 95% bootstrap confidence intervals (1,000 iterations). Models ordered chronologically: Latent Diffusion (Dec 2021), Stable Diffusion (Aug 2022), SDXL (Jul 2023), FLUX (Aug 2024), FLUX-Krea (Jul 2025). All comparisons significant at $p < 0.01$.

Our results show that distributional distinctiveness does not vanish as models advance—it *increases*. Figure 14 shows MMD^2 values rising from 0.078 [0.076, 0.084] for Latent Diffusion to 0.125 [0.121, 0.133] for Stable Diffusion to 0.126 [0.123, 0.132] for SDXL to 0.167 [0.164, 0.174] for FLUX to 0.169 [0.162, 0.179] for FLUX-Krea—more than doubling despite dramatic improvements in perceptual quality. The 95% bootstrap confidence intervals confirm that these differences are

not artifacts of sampling variability: the progression from LD to SD to FLUX represents statistically reliable increases in distinctiveness, while FLUX and FLUX-Krea are indistinguishable from each other (overlapping CIs).

Figure 15: Evolution of Human-AI Distributional Distinctiveness (Mean Across Styles)

Note: Mean MMD^2 computed separately within each of the ten artistic styles, then averaged. This within-style analysis controls for genre confounds and uses smaller per-style sample sizes, yielding higher absolute magnitudes than the pooled analysis. The monotonic increase across model generations is robust to this methodological variation.

To confirm that this pattern is not driven by a subset of styles, we also compute MMD^2 within each of the ten artistic styles separately and report the mean (Figure 15). The trajectory is qualitatively identical: 0.16 (LD) $\rightarrow$ 0.23 (SD) $\rightarrow$ 0.24 (SDXL) $\rightarrow$ 0.29 (FLUX) $\rightarrow$ 0.30 (FLUX-Krea). While absolute magnitudes differ from the pooled analysis (within-style comparisons have smaller sample sizes, yielding higher variance and higher point estimates), the monotonic increase is robust.

6.7.1 Replication on a Single-Artist Corpus: Monet's Water Lilies

The AI-ArtBench analysis pools human artworks across many artists and periods. To test whether our findings generalize to a more focused setting—and to address the possibility that cross-artist

heterogeneity drives the results—we replicate the evolution analysis on a single-artist corpus: Claude Monet's Water Lilies series.

We assembled a dataset of 200 authenticated Monet Water Lilies paintings and generated 200 AI images from each of five model generations using the prompt "an oil painting of water lilies in the style of Claude Monet." This design isolates the effect of generative modeling from artistic diversity: all human works share a single artist, subject, and style, while all AI works target the same stylistic goal.
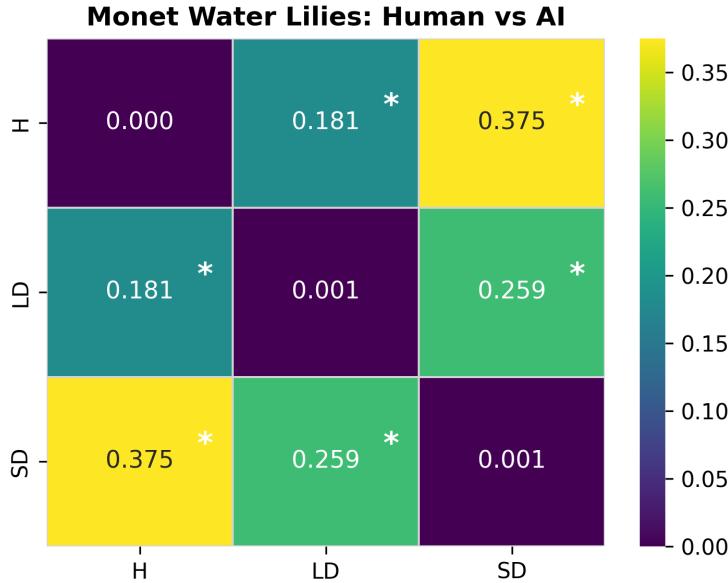

Figure 16: Monet Water Lilies: MMD Heatmap with Negative Controls

Note: MMD^2 matrix comparing Human (Monet originals), AI (LD), and AI (SD). Diagonal elements (within-source comparisons) serve as negative controls; off-diagonal elements (cross-source comparisons) test for distributional distinctiveness. Asterisks indicate $p < 0.01$. The near-zero diagonal values confirm that the method does not detect spurious differences within homogeneous sources.

Figure 16 presents the MMD heatmap for the Monet corpus. Critically, the diagonal elements (within-source comparisons: Human-A vs Human-B, AI-LD-A vs AI-LD-B, AI-SD-A vs AI-SD-B) yield near-zero MMD^2 values and are non-significant at $\alpha = 0.01$. This validates our negative controls: the method does not detect differences where none exist. Meanwhile, all off-diagonal (cross-source) comparisons are highly significant, with Human vs AI (SD) yielding $MMD^2 = 0.375$ and Human vs AI (LD) yielding $MMD^2 = 0.181$.

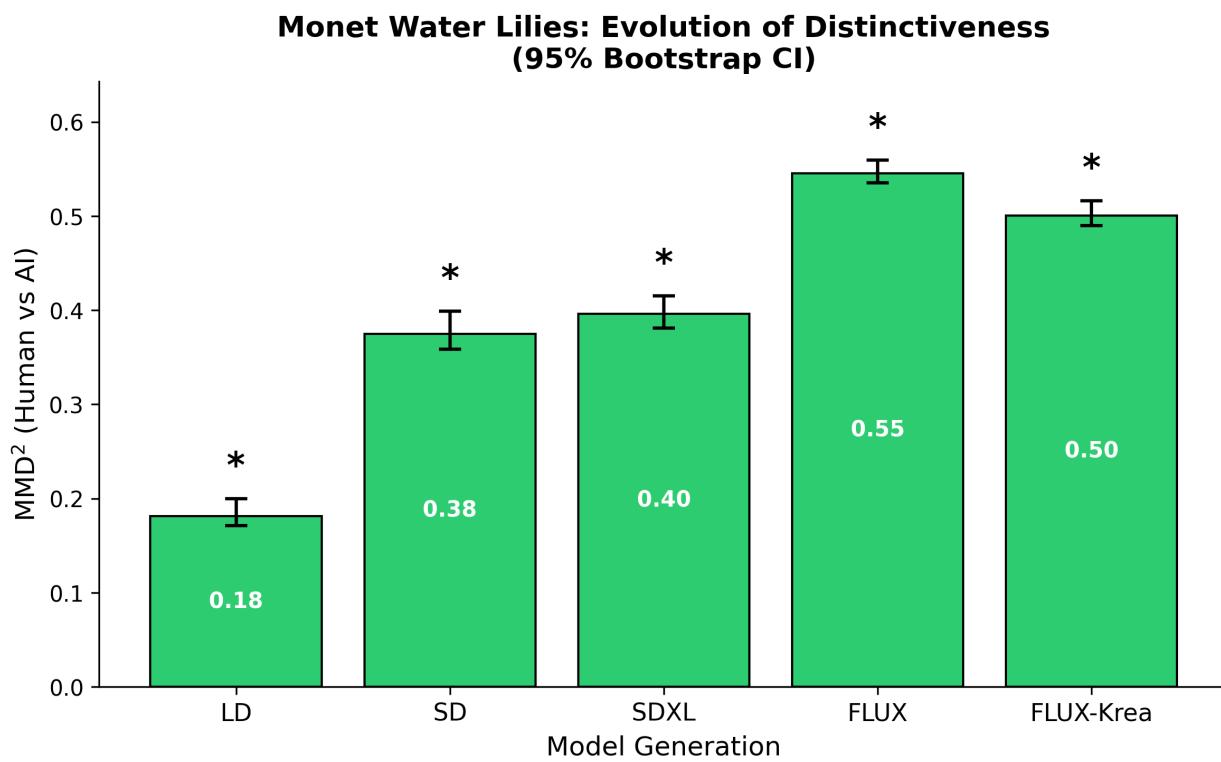The evolution analysis on this single-artist corpus confirms and amplifies the main finding

Figure 17: Monet Water Lilies: Evolution of Distributional Distinctiveness

Note: MMD^2 between Monet's Water Lilies paintings and AI-generated imitations across five model generations. Error bars indicate 95% bootstrap confidence intervals (1,000 iterations). All comparisons significant at $p < 0.01$.

(Figure 17). MMD^2 rises from 0.181 [0.171, 0.200] for Latent Diffusion to 0.375 [0.359, 0.399] for Stable Diffusion to 0.396 [0.381, 0.415] for SDXL to 0.545 [0.535, 0.559] for FLUX—more than tripling. The confidence intervals do not overlap between adjacent model generations (except SD and SDXL), confirming that the increases are statistically reliable.

Notably, FLUX-Krea yields $\mathrm{MMD}^2 = 0.501$ [0.490, 0.516], which is reliably *lower* than vanilla FLUX (CIs do not overlap). This finding is unique to the Monet corpus and was not observed in the pooled AI-ArtBench analysis, where FLUX and FLUX-Krea showed comparable distinctiveness. The difference likely reflects FLUX-Krea's design: it was fine-tuned on curated aesthetic datasets to better capture artistic styles.[41] When the target is a specific artistic tradition (Monet's Impressionism), this fine-tuning appears to reduce—but not eliminate—distributional distinctiveness: the fine-tuned model remains highly distinguishable from Monet's originals with MMD^2 values exceeding those of earlier model generations.

This Monet replication provides several important insights. First, the increasing distinctiveness over model generations is not an artifact of cross-artist heterogeneity in the human reference set; it persists when the reference is a single artist's oeuvre. Second, the validated negative controls (diagonal near-zero) confirm that the method's specificity holds in a focused setting. Third, the FLUX-Krea finding suggests that targeted fine-tuning can partially close the gap with specific artistic traditions—a finding with potential implications for copyright's substantial similarity analysis.

6.8 The Perceptual Paradox

Our central finding is that AI models exhibit "interpolative distinctiveness": they produce outputs that are semantically novel yet perceptually familiar. To probe the nature of this distinctiveness, we compare MMD scores across three embedding spaces that differ systematically in their relationship to AI-generated imagery:

1. **CLIP (ViT-H-14):** A contrastive vision-language model trained on dfn5b, a curated dataset

---

[41] *See* https://www.krea.ai/blog/flux-krea-open-source-release.

of image-text pairs scraped from the web prior to the widespread deployment of generative AI. This embedding space is *naive* to AI-generated content—it represents a purely human-centric semantic topology.

2. **DreamSim:** A perceptual similarity metric explicitly trained on synthetic images generated by text-to-image models, then calibrated to predict human perceptual similarity judgments (Fu et al. 2023). This embedding is *aware* of AI-generated imagery but is optimized to align with human perception, placing it at an intermediate position between semantic and generative representations.

3. **Stable Diffusion VAE:** The variational autoencoder from Stable Diffusion, which compresses images into the $64 \times 64 \times 4$ latent space where the diffusion process operates (Rombach et al. 2022). This is the *native generative space*—the representation in which AI outputs are literally constructed. By design, successful generation requires AI outputs to occupy the same latent manifold as human art.

These three embeddings form a spectrum from "AI-naive" (CLIP) through "AI-aware but human-calibrated" (DreamSim) to "AI-native" (VAE). If distinctiveness is a genuine property of AI outputs rather than an artifact of the measurement space, all three embeddings should detect significant differences. However, the optimization objective of each embedding suggests that the *magnitude* should vary systematically. Because diffusion models operate entirely within their VAE latent space—and would fail to generate coherent outputs if they strayed from it—we expect this embedding to show the greatest distributional overlap (lowest MMD). Conversely, CLIP represents the semantic manifold of human creation; if AI outputs are indeed "interpolative"—occupying sparse regions of the creative space between human concepts—they should appear as outliers to an AI-naive observer, yielding the highest MMD. DreamSim, by penalizing differences that humans ignore, should dampen this semantic signal, producing intermediate distinctiveness.

The empirical results confirm this prediction with striking consistency (Figure 18). Averaging across all 10 artistic styles, the Human vs. AI (SD) comparison yields mean $\text{MMD}^2 = 0.235$
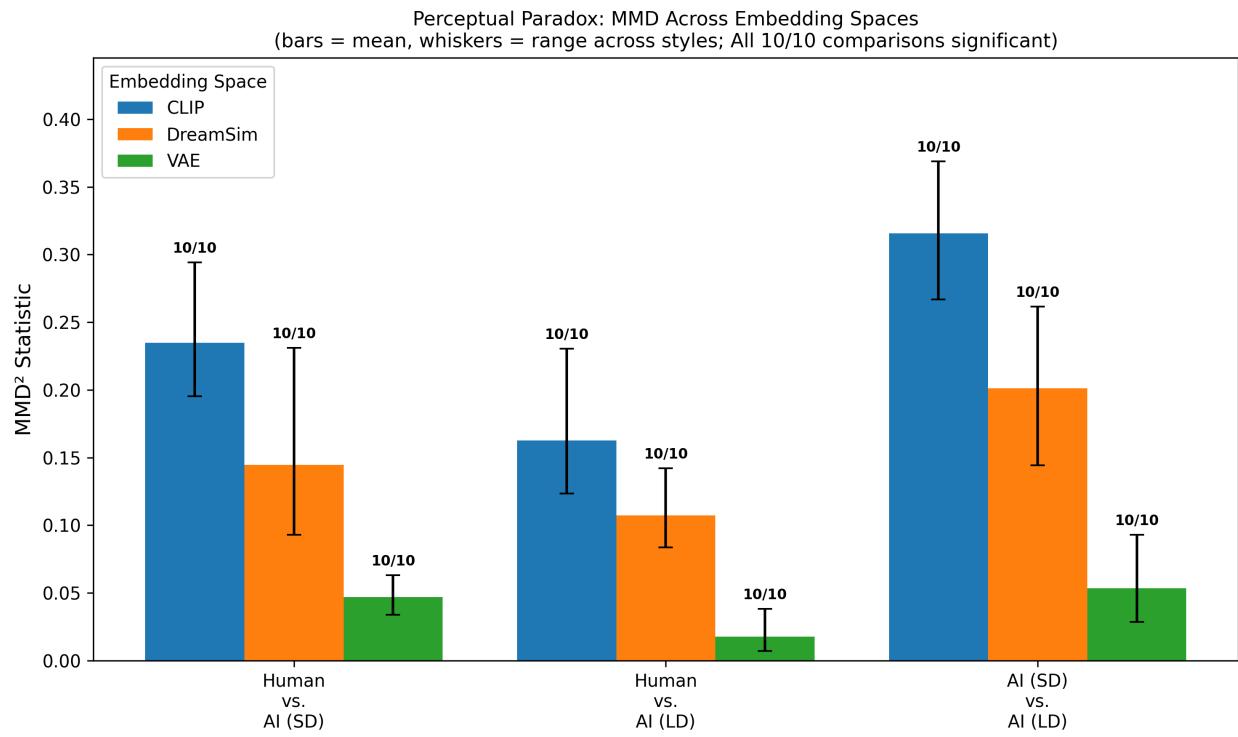
Figure 18: MMD Across Embedding Spaces: The Embedding Awareness Spectrum

Note: Bars show mean MMD^2 across 10 artistic styles; error bars indicate the range (min–max) across styles. All 90 comparisons (3 embeddings $\times$ 3 category pairs $\times$ 10 styles) achieved statistical significance ($p < 0.01$), as indicated by the "10/10" labels.

for CLIP, 0.145 for DreamSim, and 0.047 for VAE—a monotonic decrease along the AI-awareness spectrum. The same ordering holds for Human vs. AI (LD): CLIP (0.163) > DreamSim (0.107) > VAE (0.018). Yet despite this variation in magnitude, *all* 90 comparisons achieve statistical significance ($p < 0.01$), with most reaching $p = 0.002$—the minimum possible with 500 permutations. This uniformity arises because the permutation test operates *within* each embedding space: it asks whether the observed distance is extreme relative to chance variation in that same representation, not whether it exceeds some absolute threshold. The embedding choice thus affects the *magnitude* of measured distinctiveness but not whether it is *detectable.* Even in VAE space, where the generative model is designed to produce outputs that fit the latent manifold, the distributional signature remains statistically unambiguous across all styles.

This gradient of distances illuminates the nature of AI creativity. The fact that distinctiveness is *largest* in CLIP—an embedding trained exclusively on human-created imagery—suggests that AI outputs are genuine outliers in the semantic space of human creativity. They occupy regions that human artists have not densely populated. The fact that distinctiveness is *smallest* in the VAE— the space where AI outputs are constructed—reflects the design objective of generative models: to produce samples that are distributionally similar to the training data in latent space. DreamSim's intermediate position confirms that when calibrated to human perception, AI outputs appear more similar to human art than pure semantic analysis would suggest, yet remain distinguishable.

For copyright's substantial similarity analysis, this finding cuts both ways. The robust semantic distinctiveness (CLIP) supports claims of independent creation—AI outputs are not mere copies but occupy distinct regions of creative space. Yet the reduced distinctiveness in perceptually-calibrated space (DreamSim) explains why human observers struggle to distinguish AI from human art: the features humans attend to—foreground objects, composition, color, and layout (Fu et al. 2023)—are precisely those where generative models excel at mimicry. The MMD framework reveals what human perception misses: a systematic distributional signature that persists across representational choices.

7 Discussion

Our successful validation across three distinct domains—handwritten digits, patent abstracts, and AI-generated art—demonstrates the method's versatility across modalities. Substantively, these findings provide evidence that generative models do not operate as mere regurgitators of their training data. By demonstrating that AI-generated art is statistically distinct in distribution from human-created art, we identify a phenomenon of "interpolative distinctiveness" that is difficult to reconcile with mechanical regurgitation. If generative models were merely resampling training data, their output distributions would be expected to converge to the human baseline; instead, they diverge significantly. Moreover, the magnitude of this distinctiveness is probative: it suggests the divergence represents a degree of semantic separation comparable to the 'transformative' leaps recognized between distinct genres of human creativity.

Crucially, this statistical separation occurs even where human perception fails: the same AI outputs that are distributionally distinct are often perceptually indistinguishable from human art. This conjunction is the crux of the evidence against the regurgitation hypothesis. Distributional distinctiveness alone does not suffice; a random noise generator would be statistically distinct from human art yet devoid of expression. Perceptual indistinguishability alone does not suffice; it could reflect the successful compression and reproduction of training data. However, the observation that AI outputs are simultaneously distributionally novel yet semantically human-like suggests a mechanism of interpolative creativity. The models are not merely retrieving existing data points but are recombining learned patterns to generate outputs that occupy a distinct, yet semantically coherent, topological region of the creative space.

The shift from item-level to process-level analysis resolves the "infinite cardinality" problem inherent in generative AI. While traditional doctrines rely on pairwise comparisons mediated by human proxies, such methods cannot scale to unbounded output spaces. By measuring the distance between distributions, our framework allows courts and IP offices to evaluate the generative process itself. Moreover, because the method is training-free and highly sample-efficient,

it aligns with the evidentiary realities of litigation, enabling rigorous assessment even when proprietary model weights or massive training sets are inaccessible (Table 8).

Table 8: Summary of Data Efficiency: Minimum Sample Sizes for 95% Statistical Power ($\alpha = 0.01$)

Domain	Comparison Type	Typical MMD^2	N (per group)
MNIST (Images)	All digit pairs	0.81–1.22	5–6
Patents (Text)	Distinct Fields (C vs. H)	0.72	7
	Related Fields (A vs. C)	0.37	15
AI Art (Images)	High Divergence (Expressionism)	0.88	6
	Low Divergence (Art Nouveau)	0.79	6

Note: N = samples per group to reject the null with probability > 0.95. Patent sections: A = Human Necessities, C = Chemistry, H = Electricity. MNIST digit pairs all exhibit high distinctiveness; the range reflects the full off-diagonal MMD matrix.

This formalization transforms distinctiveness from a subjective gestalt impression into a form of testable empirical evidence characterized by known error rates—key factors in admissibility analyses such as *Daubert*.[42] Our framework satisfies these criteria through permutation testing, which provides exact Type I error control independent of the underlying data distribution. This allows the fact-finder to select a significance level (α) that explicitly reflects the tolerance for false positives. Rather than relying on opaque intuition, this parameter allows for a transparent calibration of evidentiary certainty that can be justified in relation to the applicable standard of proof. By converting raw semantic distances into probabilistic inferences, the method integrates computational rigor with the procedural demands of legal adjudication.

These capabilities offer specific utility across intellectual property doctrines. In trademark, the method can quantify the distinctiveness of a brand's visual footprint, providing evidence regarding the distance of a generative branding process from existing commercial symbols.[43] In copyright, it provides objective evidence of "probabilistic originality," supporting the "independent creation" prong of the *Feist* test[44] by demonstrating that a work is not a mechanical

---

[42]Daubert v. Merrell Dow Pharms., Inc., 509 U.S. 579, 593–94 (1993) (establishing that the admissibility of scientific evidence depends on factors including testability and known error rates).

[43]*See Abercrombie*, 537 F.2d at 9.

[44]Feist Publ'ns, Inc. v. Rural Tel. Serv. Co., 499 U.S. 340, 345 (1991) (holding that originality requires independent creation and a "modicum of creativity").

reproduction of the training data.[45] In patent, it offers quantitative evidence relevant to non-obviousness, measuring the "generative distance" of the claimed generative process from the prior art.[46] Here, we emphasize that this metric operationalizes the *empirical* inquiry—the magnitude of difference—not the *normative* legal conclusion. While MMD provides the factual predicate, the selection of the relevant reference class, the determination of the requisite degree of difference, amongst other issues, remain matters of legal argumentation. Nothing in the method requires style-level grouping; in a concrete copyright dispute, the relevant reference class may be as narrow as a plaintiff's catalog or an artist-period corpus, and our framework applies at that granularity (see Section 6.6 and Table 8).

This distinction between item-level and process-level distinctiveness is critical for remedies. A generative process that is distributionally distinct (high MMD) but produces rare instances of memorization presents a different legal harm than a process that is distributionally indistinguishable from its training data. The former suggests a tool with specific defects—analogous to a printing press that occasionally produces a defective copy—counseling toward targeted damages for the specific infringing outputs. The latter suggests a market substitute that systematically competes with the original works, supporting broader injunctive relief or disgorgement. Thus, while the memorization audit identifies *whether* infringement occurs, the MMD magnitude informs the *extent* and *nature* of the remedy. This bifurcated framework aligns with copyright's remedial structure, which distinguishes between actual damages (tied to specific harm) and statutory damages or profits (tied to systemic conduct).

We acknowledge important limitations. The method's sensitivity depends on embedding quality; while CLIP is robust for visual art, other domains may require specialized feature extractors. Furthermore, the validity of the inference relies on representative sampling. In adversarial litigation, parties may attempt to "cherry-pick" prompts or outputs to skew the distribution; consequently, the utility of this metric in court depends on the enforcement of rigorous sampling protocols during discovery to ensure the analyzed portfolios accurately reflect the generative

---

[45]To the extent that copyright is extended to non-natural persons.
[46]*See Graham*, 383 U.S. at 17.

process. Similarly, embeddings such as CLIP inherit biases from their training corpora. CLIP was trained predominantly on Western internet imagery, potentially underrepresenting artistic traditions from other cultures. While our Perceptual Paradox analysis (Section 6.7) demonstrates that conclusions are robust across three architecturally distinct embeddings—CLIP, DreamSim, and the Stable Diffusion VAE—this does not eliminate concerns about cultural representation. Researchers applying this framework should select embeddings that counter biases relevant to their application context; when cultural representation is paramount, embeddings trained on more diverse corpora may be appropriate. We recommend triangulating across multiple complementary embeddings to ensure robustness. Finally, while a significant MMD score establishes that a model's dominant mode is not regurgitation, it is a macro-level metric. It does not—and is not designed to—rule out the possibility that specific individual outputs may reproduce training examples. Therefore, we advocate for a bifurcated evidentiary framework: MMD to adjudicate the nature of the generative process, and targeted audits to detect specific instances of potential infringement.

These limitations suggest directions for future research. Establishing domain-specific MMD thresholds that correspond to specific legal standards of proof would enhance practical applicability. As human-AI collaboration becomes the norm, methods should be developed to disentangle machine contributions from human creative input, as the current method evaluates only the composite output. Our rejection of the regurgitation hypothesis relies on the assumption that the human artworks in our dataset are representative of the relevant prior art and the employed embeddings do not yield artefacts correlated with the central inquiry. Future work should investigate the extent to which various biases, such as cultural and representational biases, affect MMD statistics, and develop principled strategies for embedding selection and bias mitigation in legal applications. Comparing AI outputs directly to other examples of training data and broader samples of human creativity would help confirm the robustness of our key findings of a perceptual paradox in AI outputs.

As the provenance of creative works grows increasingly uncertain, intellectual property law

must evolve from intuition-based tests toward principled quantitative frameworks. By grounding assessments in distributional evidence, our methodology offers a step toward ensuring that the law reflects technological realities while preserving its fundamental purpose of incentivizing innovation and creative expression.

Bibliography

Adarsh S, Ash E, Bechtold S, et al (2024) Automating Abercrombie: Machine-learning trademark distinctiveness. Journal of Empirical Legal Studies 21:826–861. https://doi.org/10.1111/jels.12398

Bender EM, Gebru T, McMillan-Major A, Shmitchell S (2021) On the dangers of stochastic parrots: Can language models be too big? In: Proceedings of the 2021 ACM conference on fairness, accountability, and transparency. pp 610–623

Berlinet A, Thomas-Agnan C (2004) Reproducing kernel hilbert spaces in probability and statistics. Springer, New York, NY

Bińkowski M, Sutherland DJ, Arbel M, Gretton A (2018) Demystifying MMD GANs. In: International conference on learning representations (ICLR)

Bridy A (2012) Coding creativity: Copyright and the artificially intelligent author. Stanford Technology Law Review 2012:1–28

Bubeck S, Chandrasekaran V, Eldan R, et al (2023) Sparks of artificial general intelligence: Early experiments with GPT-4. arXiv preprint arXiv:230312712. https://doi.org/10.48550/arXiv.2303.12712

Byron TM (2006) Tying up Feist's loose ends: A probability theory of copyrightable creativity. Wake Forest Intellectual Property Law Journal 7:45–95

Carlini N, Ippolito D, Jagielski M, et al (2023) Quantifying memorization across neural language models. In: The eleventh international conference on learning representations (ICLR)

Chalkidis I, Kampas D (2019) Deep learning in law: Early adaptation and legal word embeddings trained on large corpora. Artificial Intelligence and Law 27:171–198. https://doi.org/10.1007/s10506-018-9238-9

Chang K, Cramer M, Soni S, Bamman D (2023) Speak, memory: An archaeology of books known to ChatGPT/GPT-4. In: Proceedings of the 2023 conference on empirical methods in natural language processing. Association for Computational Linguistics, pp 7312–7327

Chesterman S (2025) Good models borrow, great models steal: Intellectual property rights and generative AI. Policy and Society 44:23–37. https://doi.org/10.1093/polsoc/puae006

Chiba-Okabe H, Su WJ (2024) Tackling GenAI copyright issues: Originality estimation and genericization. arXiv preprint arXiv:240603341. https://doi.org/10.48550/arXiv.2406.03341

Diakopoulos N (2023) Finding evidence of memorized news content in GPT models. Generative AI in the Newsroom

Fu S, Tamir N, Sundaram S, et al (2023) Dreamsim: Learning new dimensions of human visual similarity using synthetic data. arXiv preprint arXiv:230609344. https://doi.org/10.48550/arXiv.2306.09344

Ginsburg JC, Budiardjo LA (2019) Authors and machines. Berkeley Technology Law Journal 34:343. https://doi.org/10.15779/Z38SF2MC24

Goodfellow I, Pouget-Abadie J, Mirza M, et al (2014) Generative adversarial nets. In: Advances in neural information processing systems. pp 2672–2680

Gretton A, Borgwardt KM, Rasch MJ, et al (2012) A kernel two-sample test. Journal of Machine Learning Research 13:723–773

Hain DS, Jurowetzki R, Buchmann T, Wolf P (2022) A text-embedding-based approach to measuring patent-to-patent technological similarity. Technological Forecasting and Social Change 177:121559. https://doi.org/10.1016/j.techfore.2022.121559

Helmers L, Horn F, Biegler F, et al (2019) Automating the search for a patent's prior art with a full text similarity search. PLOS ONE 14:e0212103. https://doi.org/10.1371/journal.pone.0212103

Heusel M, Ramsauer H, Unterthiner T, et al (2017) GANs trained by a two time-scale update rule converge to a local nash equilibrium. In: Advances in neural information processing systems

Ji Z, Lee N, Frieske R, et al (2023) Survey of hallucination in natural language generation. ACM Computing Surveys 55:1–38 (Article 248). https://doi.org/10.1145/3571730

Kim J-H, Kim Y, Lee J, et al (2022) Mutual information divergence: A unified metric for multimodal generative models. In: Advances in neural information processing systems (NeurIPS). pp 35072–35086

Lake BM, Baroni M (2023) Human-like systematic generalization through a meta-learning neural network. Nature 623:115–121

LeCun Y, Bottou L, Bengio Y, Haffner P (1998) Gradient-based learning applied to document recognition. Proceedings of the IEEE 86:2278–2324. https://doi.org/10.1109/5.726791

Lemley MA (2023) How generative AI turns copyright law on its head. SSRN Electronic Journal. https://doi.org/10.2139/ssrn.4517702

Liao P, Li X, Liu X, Keutzer K (2022) The ArtBench dataset: Benchmarking generative models with artworks. arXiv preprint arXiv:220611404. https://doi.org/10.48550/arXiv.2206.11404

Lin E, Peng Z, Fang Y (2024) Evaluating and enhancing large language models for novelty assessment in scholarly publications. arXiv preprint arXiv:240916605. https://doi.org/10.48550/arXiv.2409.16605

Lin W, Yu W, Xiao R (2023) Measuring patent similarity based on text mining and image recognition. Systems 11:294. https://doi.org/10.3390/systems11060294

McCoy RT, Smolensky P, Çelikyilmaz A, et al (2023) How much do language models copy from their training data? Evaluating linguistic novelty in text generation using RAVEN. Transactions of the Association for Computational Linguistics 11:652–670. https://doi.org/10.1162/tacl_a_00567

McInnes L, Healy J, Melville J (2018) UMAP: Uniform manifold approximation and projection for dimension reduction. arXiv preprint arXiv:180203426. https://doi.org/10.48550/arXiv.1802.03426

Mikolov T, Chen K, Corrado G, Dean J (2013) Efficient estimation of word representations in vector space. arXiv preprint arXiv:13013781. https://doi.org/10.48550/arXiv.1301.3781

Muandet K, Fukumizu K, Sriperumbudur B, Schölkopf B (2017) Kernel mean embedding of distributions: A review and beyond. Foundations and Trends® in Machine Learning 10:1–141. https://doi.org/10.1561/2200000060

Mukherjee A, Chang HH (2023) Managing the creative frontier of generative AI: The novelty–usefulness tradeoff. California Management Review Insights

Naeem MF, Oh SJ, Uh Y, et al (2020) Reliable fidelity and diversity metrics for generative models. In: Proceedings of the 37th international conference on machine learning. PMLR, pp 7176–7185

Nasr M, Carlini N, Hayase J, et al (2023) Scalable extraction of training data from (production) language models. arXiv preprint arXiv:231117035. https://doi.org/10.48550/arXiv.2311.17035

Phipson B, Smyth GK (2010) Permutation p-values should never be zero: Calculating exact p-values when permutations are randomly drawn. Statistical Applications in Genetics and Molecular Biology 9:Article 39. https://doi.org/10.2202/1544-6115.1585

Radford A, Kim JW, Hallacy C, et al (2021) Learning transferable visual models from natural language supervision. In: Proceedings of the 38th international conference on machine learning. PMLR, pp 8748–8763

Roca T, Roman AC, Vega JT, et al (2025) How good are humans at detecting AI-generated images? Learnings from an experiment

Rombach R, Blattmann A, Lorenz D, et al (2022) High-resolution image synthesis with latent

diffusion models. In: Proceedings of the IEEE/CVF conference on computer vision and pattern recognition. pp 10684–10695

Šavelka J, Ashley KD (2022) Legal information retrieval for understanding statutory terms. Artificial Intelligence and Law 30:245–289

Shawe-Taylor J, Cristianini N (2004) Kernel methods for pattern analysis. Cambridge University Press

Shibayama S, Yin D, Matsumoto K (2021) Measuring novelty in science with word embedding. PLOS ONE 16:e0254034. https://doi.org/10.1371/journal.pone.0254034

Silva RSR, Lotfi A, Ihianle IK, et al (2024) ArtBrain: An explainable end-to-end toolkit for classification and attribution of AI-generated art and style. arXiv preprint arXiv:241201512. https://doi.org/10.48550/arXiv.2412.01512

Solatorio AV (2024) GISTEmbed: Guided in-sample selection of training negatives for text embedding fine-tuning

Somepalli G, Singla V, Goldblum M, et al (2023) Diffusion art or digital forgery? Investigating data replication in diffusion models. In: Proceedings of the IEEE/CVF conference on computer vision and pattern recognition. pp 6048–6058

Sriperumbudur BK, Gretton A, Fukumizu K, et al (2010) Hilbert space embeddings and metrics on probability measures. Journal of Machine Learning Research 11:1517–1561

Stammbach D, Ash E (2021) Docscan: Unsupervised text classification via learning from neighbors. arXiv preprint arXiv:210504024. https://doi.org/10.48550/arXiv.2105.04024

Steinwart I, Christmann A (2008) Support vector machines. Springer Science & Business Media

Vermont S (2012) The sine qua non of copyright is uniqueness, not originality. Texas Intellectual Property Law Journal 20:327–386

Wang Z, Bovik AC, Sheikh HR, Simoncelli EP (2004) Image quality assessment: From error visibility to structural similarity. IEEE Transactions on Image Processing 13:600–612. https://doi.org/10.1109/TIP.2003.819861

Wang Z, Farnia F, Lin Z, et al (2025) On the distributed evaluation of generative models. In: Proceedings of the IEEE/CVF international conference on computer vision (ICCV) workshops. pp 7644–7653

Westermann H, Šavelka J, Walker VR, et al (2020) Sentence embeddings and high-speed similarity search for fast computer assisted annotation of legal documents. In: Legal knowledge and information systems (JURIX 2020). IOS Press, pp 164–173

Xu H, Ashley KD (2025) Label-free distinctiveness: Building a continuous trademark scale via synthetic anchors. In: Proceedings of the natural legal language processing workshop 2025. pp 113–124

Zhang J, Li CT, Farnia F (2024) An interpretable evaluation of entropy-based novelty of generative models. arXiv preprint arXiv:240217287. https://doi.org/10.48550/arXiv.2402.17287

Zhang R, Isola P, Efros AA, et al (2018) The unreasonable effectiveness of deep features as a perceptual metric. In: Proceedings of the IEEE conference on computer vision and pattern recognition (CVPR). pp 586–595

A   Appendix: Implementation Details

This appendix documents a Python implementation of the distributional distinctiveness framework developed in this paper. The implementation is designed for reproducibility, extensibility, and clarity. It can serve as a foundation for researchers adapting the methodology to new domains (e.g., trademark visual distinctiveness, literary style analysis, music generation) or practitioners deploying it in legal contexts.

Repository: During peer review, the complete codebase is available at: https://osf.io/%5BIN SERT_PLACEHOLDER_LINK%5D. Upon acceptance, this will be permanently archived with a DOI.

A.1   Architecture Overview

The codebase follows a modular architecture with a domain-agnostic statistical engine (domain-agnostic) separated from domain-specific pipelines (data loading, embedding extraction, visualization):

```
Module 1: Shared Statistical Core
    ├── MMD computation (unbiased estimator)
    ├── Permutation test (non-parametric significance)
    └── Ablation engines (kernel, dimensionality, bandwidth, stability)

Module 2: MNIST Pipeline (validation)
Module 3: Patent Pipeline (text domain)
Module 4: AI Art Pipeline (image domain)
    ├── Category analysis (per-style MMD)
    ├── Evolution analysis (model generation trajectory)
    ├── Perceptual paradox (CLIP vs DreamSim vs VAE)
    ├── Memorization audit (item-level nearest-neighbor analysis)
    └── Robustness suite (ablations, perturbations)
Module 5: Exposition Summaries (formatted output)
Module 6: Main Execution (orchestration, configuration)
```

Extending to a new domain requires: (1) a data loader returning samples with labels, (2) an embedding extractor producing numerical vectors, and (3) calls to the shared statistical functions. The core MMD and permutation test logic remains unchanged.

A.2   Dependencies

```
# Core (required)
numpy, scipy, scikit-learn, umap-learn, matplotlib, seaborn, tqdm, joblib, pillow


# Deep Learning
torch              # All studies (LeNet for MNIST, CLIP for AI Art)
torchvision        # Data augmentation transforms, MNIST data loading
open_clip_torch    # CLIP embeddings for images
sentence_transformers  # SBERT embeddings for text


# Data
datasets           # Hugging Face datasets (Patent study)
```

```
# Optional (for extended AI Art analyses)
diffusers          # VAE latent extraction
dreamsim           # Perceptual embeddings
scikit-image       # SSIM computation for memorization audit
lpips              # Learned perceptual similarity for memorization audit

# Performance
numexpr            # Fast array expression evaluation
psutil             # Memory checking for precomputation decisions
```

A.3   Module 1: Shared Statistical Core

This module implements the theoretical framework from Section 3. All functions operate on numerical vectors (embeddings) and are agnostic to the underlying data type.

A.3.1   Core MMD Functions

- *_compute_sigma_median_heuristic(x, y)* → *float*: Computes the bandwidth parameter σ for the RBF kernel using the median heuristic: σ = median of all pairwise Euclidean distances in the combined sample. This data-driven approach automatically scales the kernel's sensitivity to the data's intrinsic dimensionality, avoiding manual tuning. The median heuristic is preferred over cross-validation because it is (a) deterministic, (b) computationally cheap, and (c) provides reasonable performance across diverse datasets without risk of overfitting to a specific comparison.
- *mmd_squared_unbiased(x, y, kernel='rbf', gamma=None)* → *float*: Computes the unbiased squared MMD estimator that has expected value zero under the null hypothesis regardless of sample size, enabling valid comparison across different n. Uses *scipy.spatial.distance.pdist*/*cdist* for efficient pairwise distance computation (computing only unique pairs) combined with *numexpr* for fast kernel evaluation. Supports both RBF kernel (default, captures all moments) and linear kernel (captures only mean difference).
- *permutation_test(x, y, R, alpha, ...)* → *(p_value, reject, lb, ub)*: Implements Algorithm 1, the non-parametric permutation test for MMD significance. Under H_0 (identical distributions), pooling and reshuffling samples should produce MMD values similar to the observed value; if the observed MMD is extreme relative to the permutation distribution, we reject H_0. R is then number of permutation iterations. With R=500, minimum attainable p-value is 1/501 ~ 0.002, sufficient for α=0.01. If *precompute* is True, the function computes the full kernel matrix once before permutations. This dramatically improves performance for large samples but requires $O(n^2)$ memory. The function automatically falls back to on-the-fly computation if memory is insufficient. *n_jobs* parallelizes permutation iterations using *joblib* with thread-based backend (avoids memory copying overhead). The function uses the conservative Monte Carlo estimator (r+1)/(R+1) where r is the count of permuted statistics $\geq$ observed. This avoids zero *p*-values and is the standard approach in permutation testing literature.

A.3.2 Shared Ablation Functions

These functions implement domain-agnostic robustness analyses, ensuring methodological consistency across studies.

- *compute_stability_analysis(x, y, dims_list, n_trials, sample_size)* → *dict*: Implements Section 4.3: evaluates how UMAP compression error propagates to the MMD statistic. For each target dimension d, computes MMD in both full and reduced spaces across multiple trials, returning the mean and standard deviation of the absolute deviation. UMAP is fit on the pooled sample ($X \cup Y$), not separately on each group. Fitting separately would artificially inflate differences by allowing each group to find its own optimal subspace.
- *compute_kernel_ablation(x, y, sample_sizes, n_trials, R, alpha, n_jobs)* → *dict*: Compares RBF vs. Linear kernel rejection rates. The Linear kernel MMD measures only centroid distance; the RBF kernel captures higher-order distributional structure. If both kernels reject at similar rates, distinctiveness is driven by mean shift; if RBF substantially outperforms Linear, the distributions differ in variance or shape.
- *compute_dimensionality_ablation(x, y, dims_list, sample_sizes, n_trials, R, alpha, n_jobs)* → *dict*: Tests whether the statistical conclusion (reject/fail-to-reject) is stable under aggressive dimensionality reduction. Uses paired sampling: for each (n, trial), the same sample is tested across all dimensions, enabling clean comparison. UMAP requires the target dimension to be strictly less than the pooled sample size ($d < 2n$). When this constraint is violated, the function returns NaN rather than failing, allowing partial results. For example, reducing to $d = 32$ dimensions requires at least $n = 17$ samples per group (34 total).
- *compute_bandwidth_ablation(x, y, sigma_multipliers, sample_sizes, ...)* → *dict*: Tests robustness to the bandwidth hyperparameter by scaling the median-heuristic σ by specified multipliers (e.g., 0.5×, 1.0×, 2.0×). A "plateau of significance" (high rejection across all multipliers) indicates the result is not an artifact of specific tuning. The baseline σ is estimated from a larger fixed sample (default n=200) independent of the test sample size, reducing noise in the bandwidth estimate.

A.4 Module 2: MNIST Study

Validates the framework using MNIST digits where ground truth is known (e.g., digit 3 ≠ digit 5). For robustness analyses, the digit pair with the lowest off-diagonal MMD^2 (hardest to distinguish) is automatically selected at runtime, providing the most conservative test. This module demonstrates the methodology in a controlled setting before applying it to legally relevant domains. The implementation uses PyTorch for neural network training and embedding extraction.

A.4.1 Model Architecture

The *LeNet5* class implements the classic convolutional architecture as a PyTorch *nn.Module*:

```
Input (1×28×28) → Conv(6, 5×5) → AvgPool(2×2) → Conv(16, 5×5) → AvgPool(2×2) →
FC(256→120) → Dropout(0.1) → FC(120→84) [embedding] → Dropout(0.1) → FC(84→10)
```

The 84-dimensional embedding layer (fc2) serves as the feature representation for MMD analysis. Embeddings are extracted via the model's *forward(x, extract_embeddings=True)* method, which returns activations before the final classification layer.

A.4.2 Data Augmentation

The *AugmentedDataset* class wraps PyTorch's *Dataset* to apply transforms per-sample rather than to batched tensors. This is necessary because torchvision applies identical random transforms to all images in a batch; per-sample application ensures independent randomization. Augmentation uses a single *RandomAffine* transform combining rotation (±10°), translation (±10%), and scaling (0.9×–1.1×) in one interpolation step, reducing artifacts compared to chained transforms.

A.4.3 Core Functions

- *mnist_load_and_prepare_data()*: Loads MNIST via torchvision, normalizes pixels to [0,1], reshapes for CNN input.
- *mnist_build_lenet5_model()*: Factory function returning a LeNet5 *nn.Module* instance with 84-dimensional embedding layer.
- *mnist_train_model(...)*: Trains with data augmentation, early stopping, and checkpointing. Uses Adam optimizer with cross-entropy loss. Automatic device selection prioritizes CUDA (NVIDIA GPU), then MPS (Apple Silicon), then CPU.
- *mnist_extract_embeddings(...)*: Extracts 84-dim vectors (float32 precision for GPU/MPS compatibility) from the trained model's penultimate layer with the model in evaluation mode (dropout disabled).
- *mnist_compute_mmd_matrix(...)*: Computes 10×10 MMD matrix for all digit pairs. Diagonal entries use split-half negative control: each digit class is split into two disjoint halves, and MMD is computed between them. Under H_0, these should yield non-significant results.
- *mnist_compute_rejection_rates(...)*: Estimates statistical power across sample sizes via Monte Carlo trials.

A.4.4 Visualization

- *mnist_plot_mmd_heatmap(...)*: Heatmap of MMD values with significance markers. Negative values (possible due to unbiased estimator variance) are clamped to zero for visualization only.
- *mnist_plot_rejection_rates(...)*: Line plot of rejection rate vs. sample size.
- *mnist_plot_stability_curve(...)*: Plots approximation error vs. UMAP dimensions (Section 4.3).

A.4.5 Robustness Suite

- *mnist_run_robustness_suite(...)*: Orchestrates all ablations (stability, kernel, dimensionality, representation, bandwidth, perturbation) and saves results. Generates *mnist_perturbation_results.pkl* (serialized perturbation data) and *mnist_ablation_tables.txt* (formatted tables for all ablation results).
- *mnist_compute_representation_ablation(...)*: Compares raw 784-dim pixels vs. learned 84-dim embeddings. For structurally simple objects like digits, raw pixels should work comparably—validating that MMD functions correctly even without sophisticated embeddings.

- *mnist_perturbation_analysis(...)*: Tests robustness to Gaussian noise (parameterized by SNR) and grid watermarks (parameterized by SWR) using a paired sample design (the same images are used for clean and perturbed conditions, projected jointly via UMAP).
- *mnist_perturbation_table_combined(...)*: Generates a consolidated perturbation table showing ΔMMD and *p*-values across multiple digits (used in manuscript Table 2).
- *mnist_save_ablation_tables(...)*: Prints and saves formatted tables for all ablation results (kernel, bandwidth, dimensionality, representation, perturbation). Tables are both printed to stdout for monitoring and saved to *mnist_ablation_tables.txt* for reference during manuscript writing.

A.5 Module 3: Patent Study

Validates the framework on text using patent abstracts from different IPC sections. Demonstrates that the methodology generalizes beyond images to semantic text embeddings.

A.5.1 Core Functions

- *patent_load_dataset(...)*: Loads from *ccdv/patent-classification* via Hugging Face. Filters for sections A (Human Necessities), C (Chemistry), H (Electricity). Cleans text using regex to remove explicit class labels that could cause leakage. Collects 2× samples to enable split-half negative controls.
- *patent_extract_embeddings(...)*: Extracts 384-dim embeddings using SentenceTransformers (*GIST-small-Embedding-v0*, with *all-MiniLM-L6-v2* as fallback). Embeddings are L2-normalized for RBF kernel stability.
- *patent_compute_mmd_matrix(...)* and *patent_compute_rejection_rates(...)*: Standard MMD analysis with split-half negative controls on diagonal.

A.5.2 Visualization and Output

- *patent_plot_mmd_heatmap(...)* and *patent_plot_rejection_rates(...)*: Analogous to MNIST visualizations.
- *patent_save_summary_tables(...)*: Prints and saves formatted summary tables (MMD matrix, *p*-values, rejection rates) to *patent_summary_tables.txt*.

A.6 Module 4: AI Art Study

The primary legal application: comparing human-created art to AI-generated art across multiple models and artistic styles.

A.6.1 Data Loading and Embedding

Internal helper functions (*_slugify, _extract_style_from_original_class, _filter_embeddings_by_style*) handle filename normalization and style-based filtering.

- *art_load_dataset(...)*: Loads images from an AI-ArtBench-like directory structure with *stratified sampling* by artistic style. The *max_images_per_style* parameter (default 250) ensures

equal representation of each style within each category, yielding 2,500 images per category (250 × 10 styles). The *categories_map* parameter maps target categories to folder prefixes. Supports optional manifest presence check for evolution analysis.

- *art_extract_clip_embeddings(...)*: Extracts 1024-dim semantic embeddings using CLIP (ViT-H-14-quickgelu, dfn5b pretrained). CLIP captures high-level semantic and stylistic features suitable for art comparison.

A.6.2 Category-Level Analysis (Primary Pipeline)

The primary AI Art analysis operates at the style level, computing Human vs. AI distinctiveness within each artistic movement:

- *art_compute_category_mmd_analysis(...)*: Iterates through styles, computes 3×3 MMD matrix (Human × AI(SD) × AI(LD)) per style.
- *art_compute_category_rejection_rates(...)*: Computes per-style rejection rate curves.
- *art_compute_category_summary(...)*: Ranks styles by MMD (convergence ranking), identifies fast/median/slow converging styles via terciles, computes threshold sample sizes for 95% power.

A.6.3 Category-Level Visualization

- *art_plot_category_heatmaps(...)*: Grid of per-style 3×3 heatmaps (2×5 layout for 10 styles).
- *art_plot_category_rejection_rates(...)*: Rejection rate vs. sample size, one line per style.
- *art_plot_category_mmd_comparison(...)*: Grouped bar chart comparing Human-AI(SD) and Human-AI(LD) MMD across styles.
- *art_print_category_exposition_summary(...)*: Formatted text summary of category-level findings.

A.6.4 Evolution Analysis (Section 6.5)

- *art_compute_evolution_analysis(...)*: Computes MMD between a human baseline and each model generation (LD → SD → SDXL → FLUX → FLUX-Krea). The human baseline sample is fixed to ensure that changes in MMD reflect model evolution, not sampling variation in the human reference. SDXL and FLUX images were generated using *generate_images.py* with consistent prompts matching AI-ArtBench style categories. For MMD testing, comparisons use up to 500 samples per group (controlled by *sample_cap*).
- *art_plot_evolution_curve(...)*: Line plot of MMD vs. model generation.
- *art_plot_evolution_grid(...)*: Creates a 3×6 grid of exemplar images showing visual evolution across model generations (Human → LD → SD → SDXL → FLUX → FLUX-Krea) for three representative styles. Images are hand-picked and stored in *art_results/evolution_grid_images/*.

A.6.5 Perceptual Paradox Analysis (Section 6.7)

- *art_extract_vae_embeddings(...)*: Extracts 16,384-dim VAE latents (64×64×4 flattened) from *stabilityai/sd-vae-ft-mse*, the Stable Diffusion encoder fine-tuned on reconstruction loss. Tests whether distinctiveness is an artifact of the model's compression scheme.

- *art_extract_dreamsim_embeddings(...)*: Extracts embeddings from DreamSim, trained to match human perceptual judgments. Tests the "perceptual paradox": distinct in semantic space (CLIP) but indistinguishable in perceptual space (DreamSim).
- *art_compute_perceptual_paradox_by_style(...)*: The primary perceptual paradox analysis. Computes MMD for each of 10 artistic styles across 3 embedding types (CLIP, DreamSim, VAE) and 3 comparisons (Human vs AI(SD), Human vs AI(LD), AI(SD) vs AI(LD)), yielding 90 MMD values total. Returns per-style results and aggregate statistics (mean, std, min, max) with significance counts across styles.
- *art_plot_perceptual_paradox(...)*: Grouped bar chart visualizing the perceptual paradox results. Shows 3 comparison groups × 3 embedding bars per group, with error bars indicating min-max range across styles and "n/10" significance counts above each bar. Hypothesis: CLIP (AI-naive) > DreamSim (AI-aware) > VAE (AI-native).
- *art_compute_embedding_comparison(...)*: Legacy function for single-style embedding comparison. Superseded by *art_compute_perceptual_paradox_by_style()* for aggregate analysis.
- *art_plot_embedding_comparison(...)*: Grouped bar chart for single-style embedding comparison.

A.6.6   Style Comparison (Magnitude Contextualization)

- *art_compute_style_comparison(...)*: Computes MMD between pairs of human art movements (e.g., Impressionism vs. Realism). Calibrates the "legal distance": is Human-AI divergence larger or smaller than the gap between major human movements? Uses exact style matching via *_extract_style_from_original_class()* to avoid substring contamination (e.g., "realism" incorrectly matching "surrealism").

A.6.7   Robustness and Perturbation

- *art_run_robustness_suite(..., target_style=None, embeddings_raw=None, comparison_pairs=None)*: Orchestrates all ablations. If *target_style* is provided, filters to that style before analysis. The *embeddings_raw* parameter accepts raw 1024-dim CLIP embeddings for dimensionality ablation (which tests reduction from high dimensions). The *comparison_pairs* parameter accepts a list of tuples, e.g., *[('Human', 'AI (SD)'), ('Human', 'AI (LD)')]*, enabling ablations across multiple comparisons in a single call. Results are saved with pair-specific suffixes (e.g., *kernel_ablation_results_h_sd.pkl*, *kernel_ablation_results_h_ld.pkl*).
- *_comparison_pair_suffix(pair)*: Helper function that converts comparison tuples to filename suffixes, e.g., *('Human', 'AI (SD)') → '_h_sd'*.
- *art_perturbation_analysis(...)*: Tests robustness to noise and watermarks, analogous to MNIST. Uses a paired sample design with joint UMAP projection; sample size controlled by *n_samples* parameter.
- *art_perturbation_table(...)*: Generates formatted p-value tables for perturbation results (used in manuscript Table 4).
- *art_print_robustness_summary(...)*: Formatted text summary of robustness findings.
- *art_save_ablation_tables(...)*: Prints and saves formatted ablation tables (kernel, bandwidth, dimensionality, embedding comparison, perturbation) to *art_ablation_tables.txt*.

A.6.8 Memorization Audit (Item-Level Analysis)

The distributional MMD test answers whether the *process* is distinct; the memorization audit answers whether specific *outputs* exhibit suspicious similarity to training data. This bifurcated approach is legally necessary: a generative process can be distributionally novel ($Q \neq P$) while still occasionally regurgitating near-copies.

Key insight: Distributional tests average over the output space, potentially masking a small fraction of memorized outputs. If an AI model is 99% creative and 1% regurgitative, MMD will indicate "distinct," but copyright law still cares about that 1%.

- *art_compute_memorization_audit(embeddings_raw, images, categories, original_classes, config, output_dir)*: The primary memorization detection function. For each AI-generated image, finds its nearest neighbor among human images *within the same artistic style* using three complementary metrics:

    - **CLIP cosine similarity**: Semantic proximity in the 1024-dim embedding space. High similarity suggests the AI output captures the same semantic content as a human work.
    - **SSIM** (Structural Similarity Index): Pixel-level structural correspondence measuring luminance, contrast, and structure. Detects visual copying that may not register semantically.
    - **LPIPS** (Learned Perceptual Image Patch Similarity): Deep perceptual distance trained to match human similarity judgments. Bridges semantic and structural measures.

Within-style comparisons: Comparisons are constrained to the same artistic style (e.g., AI impressionist images compared only to human impressionist images). This is critical because cross-style comparisons would conflate style distance with potential copying—an AI Baroque image should not be flagged simply for being distant from human Impressionism.

Threshold establishment: The human-human baseline establishes what "normal" within-style similarity looks like. For each human image, we find its nearest neighbor among *other* human images of the same style. The 99th percentile of this distribution becomes the detection threshold for CLIP and SSIM (where higher = more similar). For LPIPS (where lower = more similar), we use the 1st percentile.

Exceedance rate: The key output metric. What percentage of AI outputs have nearest-neighbor similarity exceeding the human-human baseline threshold? An exceedance rate near 1% is expected by construction (matching the threshold percentile); rates substantially higher suggest systematic memorization.

- *art_plot_memorization_audit(audit_results)*: Generates a 3-panel histogram visualization showing the distribution of nearest-neighbor similarities for Human-Human (baseline), AI(SD)-Human, and AI(LD)-Human, with threshold lines marked. Useful for understanding the full distribution of similarity scores.

- *art_plot_memorization_exceedance_chart(audit_results)*: The primary visualization for the memorization audit. Generates a grouped bar chart showing exceedance rates across metrics (CLIP, SSIM, LPIPS) and models (SD, LD). Bar heights represent the mean exceedance rate across styles; whiskers show the min-max range. A horizontal dashed line at 1% marks

the expected baseline (since the threshold is the 99th percentile of human-human similarity, exactly 1% of human works "exceed" by construction). Rates at or below this line indicate the AI produces high-similarity outputs no more frequently than human artists.

- *art_save_memorization_audit_table(audit_results, filename)*: Saves a formatted table summarizing exceedance rates across all three metrics for both AI model types. This table provides the empirical basis for the "bifurcated inquiry" discussed in Section 2.

Legal significance: The combination of high MMD (process distinctiveness) and low exceedance rates (rare memorization) suggests a tool with occasional defects rather than a systematic copying machine. This distinction is relevant for remedies: targeted damages for specific infringements vs. broad injunctive relief for market substitution.

A.7   Module 5: Exposition Summaries

Functions that extract and format key results for academic writing:

- *print_mnist_exposition_summary(...)*: Sample size thresholds, negative control statistics, significance rates.
- *print_patent_exposition_summary(...)*: Cross-section comparisons, negative control verification.
- *art_print_category_exposition_summary(...)*: Per-style MMD values, convergence rankings, threshold sample sizes.
- *print_mnist_robustness_exposition_summary(...)*: Consolidates all MNIST ablation findings.
- *print_art_robustness_exposition_summary(...)*: Consolidates evolution and robustness findings for AI Art.

A.8   Module 6: Main Execution

A.8.1   Configuration

All parameters are centralized in the configuration section preceding the *if __name__ == "__main__"* block. Key parameters include:

- *SAMPLE_CAP = 500*: Maximum samples per class/category for MMD computations
- *PATENT_N_SAMPLES = 500*: Samples per IPC section for patent study
- *ART_MAX_IMAGES_PER_STYLE = 250*: Images per artistic style (stratified sampling)
- *R = 500*: Permutation iterations for all hypothesis tests
- *ALPHA = 0.01*: Significance level
- UMAP: 64 dimensions, cosine metric

Extended parameters are organized into configuration dictionaries (*MNIST_ROBUSTNESS_CONFIG*, *ART_ROBUSTNESS_CONFIG*, *ART_PERTURBATION_CONFIG*, *MEMORIZATION_AUDIT_CONFIG*, etc.) for clarity.

The memorization audit is controlled by:

- *RUN_MEMORIZATION_AUDIT = True*: Toggle to enable/disable the item-level analysis
- *MEMORIZATION_AUDIT_CONFIG*: Dictionary containing *threshold_percentile* (default 99) and *device* (e.g., 'mps' for Apple Silicon, 'cuda' for NVIDIA)

A.8.2 Execution Flow

1. Seed Management: *set_all_seeds(seed)* initializes NumPy, PyTorch (including CUDA if available), and Python random seeds for reproducibility. For deterministic GPU operations, the function also sets *torch.backends.cudnn.deterministic = True.*
2. Directory Setup: Creates *mnist_results/*, *patent_results/*, *art_results/*.
3. MNIST Study: Train LeNet → Extract embeddings → MMD matrix → Rejection rates → Auto-select hardest pair → Robustness suite → Save & plot.
4. Memory Cleanup: After MNIST completes, the model is deleted and GPU memory is released via *torch.cuda.empty_cache()* (NVIDIA) or *torch.mps.empty_cache()* (Apple Silicon). This ensures subsequent studies have maximum available memory.
5. Patent Study: Load & embed → MMD matrix → Rejection rates → Save & plot.
6. AI Art Study: Load & embed → Category analysis → Evolution analysis → Perceptual paradox → Memorization audit → Robustness (on representative styles) → Perturbation → Save & plot.
7. Exposition Summaries: Print formatted results for each study.

A.8.3 Automated Style Selection

To avoid running expensive ablations on all 10 styles, the script automatically selects three representative styles based on category analysis results:

- One from the *fast-converging tercile* (low MMD)
- One from the *median tercile*
- One from the *slow-converging tercile* (high MMD)

Robustness and perturbation analyses run only on these three styles.

A.8.4 Output Formats

- *.npy*: Pure numpy arrays (embeddings, MMD matrices, p-value matrices)
- *.pkl*: Python dictionaries (rejection rates, ablation results, robustness suites)
- *.npz*: Compressed numpy archives (patent embeddings dictionary)
- *.png*: All visualizations (heatmaps, line plots, bar charts)
- *.txt*: Formatted tables for reference during manuscript writing (e.g., *mnist_ablation_tables.txt*, *patent_summary_tables.txt*, *art_ablation_tables.txt*, *art_memorization_audit_table.txt*)

A.8.5 Embedding Caching

CLIP embedding extraction is computationally expensive (~30 minutes on GPU). To accelerate re-runs, the AI Art study caches embeddings with validation:

- **Cache files**: *art_clip_embeddings_raw.npy* (1024-dim), *art_clip_embeddings.npy* (64-dim UMAP-reduced), *art_categories.npy*, *art_original_classes.npy*
- **Validation**: On load, the cache is validated by checking (1) sample count matches loaded images and (2) category sets match. If validation fails, embeddings are re-extracted.

- **Cache invalidation**: Changing *RUN_EVOLUTION_ANALYSIS* or modifying the image dataset invalidates the cache automatically.

This reduces ablation-only re-runs from ~2 hours to ~30 minutes.

A.9 Extending to New Domains

To apply this framework to a new domain (e.g., trademark logos, music samples, literary texts):

1. *Write a data loader* returning *(samples, labels)* where samples can be any format your embedding extractor accepts.

2. *Write an embedding extractor* that converts samples to fixed-length numerical vectors. Choose an embedding model appropriate to your domain:

   - Images: CLIP, ResNet, domain-specific models
   - Text: SBERT, legal-specific transformers
   - Audio: wav2vec, audio spectrograms + CNN

3. *Call the shared statistical functions*:

   - *mmd_squared_unbiased(emb_A, emb_B)* for distributional distance
   - *permutation_test(emb_A, emb_B, ...)* for significance testing
   - *compute_stability_analysis(...)* and *compute_kernel_ablation(...)* for robustness checks

4. *Adapt visualization functions* or use the outputs directly for custom plots.

The statistical core (Module 1) requires no modification. Domain expertise is concentrated in the data loader and embedding extractor.